

1 **C-GEM (v 1.0): A new, cost-efficient biogeochemical model**  
2 **for estuaries and its application to a funnel-shaped system**

3

4 **C. Volta<sup>1</sup>, S. Arndt<sup>2</sup>, H.H.G. Savenije<sup>3</sup>, G.G. Laruelle<sup>1</sup> and P. Regnier<sup>1</sup>**

5

6 <sup>1</sup>Department of Earth and Environmental Sciences, Université Libre de Bruxelles, Brussels,  
7 Belgium

8 <sup>2</sup>School of Geographical Sciences, University of Bristol, Bristol, UK

9 <sup>3</sup>Water Resources Section, Department of Water Management, Delft University of  
10 Technology, Delft, The Netherlands

11 Correspondence to: C. Volta (cvolta@ulb.ac.be)

12

13 **Abstract**

14 Reactive-transport models (RTMs) are powerful tools to disentangle the complex process  
15 interplay that drives estuarine biogeochemical dynamics, to assess the quantitative role of  
16 estuaries to global biogeochemical cycles and to predict their response to anthropogenic  
17 disturbances (land-use change, climate change and water management). Nevertheless, the  
18 application of RTMs for a regional or global estimation of estuarine biogeochemical  
19 transformations and fluxes is generally compromised by their high computational and data  
20 demands. Here, we describe C-GEM (Carbon-Generic Estuary Model), a new one-  
21 dimensional, computationally efficient RTM that reduces data-requirements by using a  
22 generic, theoretical framework based on the direct relationship between estuarine geometry

1 and hydrodynamics. Despite its efficiency, it provides an accurate description of estuarine  
2 hydrodynamics, salt transport and biogeochemistry at the appropriate spatio-temporal scales.  
3 We provide a detailed description of the model, as well as a protocol for its set-up. The new  
4 model is then applied to the funnel-shaped Scheldt estuary (BE/NL), one of the best-surveyed  
5 estuarine systems in the world. Its performance is evaluated through comprehensive model-  
6 data and model-model comparison. Model results show that C-GEM captures the dominant  
7 features of the biogeochemical cycling in the Scheldt estuary. Longitudinal steady-state  
8 profiles of oxygen, ammonium, nitrate and silica are generally in good agreement with  
9 measured data. In addition, simulated, system-wide integrated reaction rates of the main  
10 pelagic biogeochemical processes are comparable with those obtained using a high-resolution,  
11 two-dimensional RTM. A comparison of fully transient simulations results with those of a  
12 two-dimensional model shows that the estuarine Net Ecosystem Metabolism (NEM) only  
13 differs by about 10%, while system-wide estimates of individual biogeochemical processes  
14 never diverge by more than 40%. A sensitivity analysis is carried out to assess the sensitivity  
15 of biogeochemical processes to uncertainties in parameter values. Results reveal that the  
16 geometric parameters LC (estuarine convergence length) and H (water depth), as well as the  
17 rate constant of organic matter degradation ( $k_{ox}$ ) exert an important influence on the  
18 biogeochemical functioning of the estuary. The sensitivity results also show that, currently,  
19 the most important hurdle towards regional or global scale applications arises from the lack of  
20 an objective framework for sediment and biogeochemical process parameterization. They,  
21 therefore, emphasize the need for a global compilation of biogeochemical parameter values  
22 that can help identify common trends and possible relationships between parameters and  
23 controlling factors, such as climate, catchment characteristics and anthropic pressure.

24

# 1 1 Introduction

2 Estuaries are important components of the morphologically complex and highly dynamic  
3 transition zone between the terrestrial environment and the ocean (e.g. Alongi, 1998;  
4 Crossland et al., 2005). In estuaries, tightly coupled hydrodynamic, geological, geochemical  
5 and biological processes interact on very different temporal and spatial scales and adjust, at  
6 different rates, to perturbations induced by a wide array of physical forcing mechanisms. As a  
7 result, a significant, but highly variable fraction of the land-derived inputs of carbon and  
8 associated bio-elements (*N, P, Si*) is chemically and biologically modified along the estuarine  
9 gradient, with likely consequences for the coastal biogeochemical dynamics and, ultimately,  
10 for global biogeochemical cycles (e.g. Jahnke, 1996; Gattuso et al., 1998; Rabouille et al.,  
11 2001; Laruelle et al., 2009; Liu et al., 2010; Arndt et al., 2011; Jiao et al., 2011; Regnier et al.,  
12 2013a; **Bauer et al, 2013**).

13 The limited number of comparative studies covering a large range of estuarine systems  
14 hampers the identification of global patterns and precludes a robust assessment of the  
15 quantitative role of estuaries to global element cycles (Borges and Abril, 2011). In addition,  
16 individual estuarine systems **reveal** tremendous internal spatial and temporal heterogeneity,  
17 making it difficult to quantify the net carbon balance for a single estuary and even more for a  
18 set of representative systems upon which regional and global estimates could rely (Bauer et  
19 al., 2013). In this context, the long tradition of research in estuarine physics provides a  
20 suitable framework for addressing the large-scale estuarine biogeochemical dynamics.  
21 Dominant features of the estuarine transport can be constrained from hydrodynamic  
22 parameters (e.g. Stommel and Farmer, 1952; Hansen and Rattray, 1966; Prandle, 1985; Jay et  
23 al., 2000) or geometrical parameters (e.g. Pritchard, 1955; Davies, 1964; Dyer, 1973; Pethick,  
24 1984; Dalrymple et al., 1992; Dürr et al., 2011), two seemingly distinct approaches which can

1 be related to one another through the interdependence between estuarine geometry and  
2 hydrodynamics (Savenije, 1992). Hence, important transport and mixing properties can be  
3 directly deduced from readily available geometric data (Savenije, 2005, 2012). Taking into  
4 account that the hydrodynamics also exerts a first-order control on the estuarine  
5 biogeochemistry (e.g. Alpine and Cloern, 1992; Friedrichs and Hofmann, 2001; Arndt et al.,  
6 2007), a logical step is to use these interdependencies to predict the biogeochemical dynamics  
7 from the main geometrical features of estuaries.

8 The tight hydrodynamic-biogeochemical coupling has already been partly recognized in the  
9 past, for instance by correlating the biogeochemical behaviour of an estuary to given  
10 hydrodynamic characteristics, such as residence time or tidal forcing (Monbet, 1992; Nixon et  
11 al., 1996; Laruelle, 2009). Yet, these correlations are based on a limited number of datasets  
12 (<40) that do not cover the diversity of estuarine systems and do not resolve their seasonal  
13 and inter-annual variability (e.g. Brion et al., 2008; Arndt et al., 2009). Such correlative  
14 approach also does not provide fundamental insights into the complex interplay of multiple  
15 reaction and transport processes in estuarine systems (Nielsen et al., 1995; Geyer et al., 2000;  
16 Arndt et al. 2009). The aim is thus to extend the approach and to develop generalized methods  
17 for up-scaling that resolve the strong spatio-temporal variability of the estuarine environment  
18 and explicitly account for the process interplay that controls the biogeochemical cycling of  
19 carbon and nutrients along the estuarine gradient.

20 Over the last three decades, increasingly complex process-based models have been applied to  
21 unravel the organic and inorganic carbon and nutrient cycles at the scale of individual  
22 estuaries (e.g. O’Kane, 1980; Soetaert and Herman, 1995; Vanderborght et al., 2002; Lin et  
23 al., 2007; Arndt et al., 2009; Cerco et al., 2010; Baklouti et al., 2011). Yet, none of these  
24 models are currently suitable for regional or global applications (Bauer et al, 2013). In

1 particular, model applications remain limited by data requirements, calibration and validation  
2 procedures as well as by high computational demand required to address **important** physical,  
3 biogeochemical and geological processes at the relevant temporal and spatial scales (Regnier  
4 et al, **2013b**). Therefore, applications at scales larger than individual, well constrained systems  
5 require simplifications to afford the treatment of a large number of estuaries, including those  
6 for which morphological, hydrodynamic and biogeochemical data are incomplete or absent. A  
7 generalization of simulation results from a representative set of systems covering contrasting  
8 climate, hydromorphology and catchment properties will ultimately provide better estimates  
9 of the quantitative contribution of estuaries to global biogeochemical cycles.

10 Here, we propose the Carbon – Generic Estuary Model (C-GEM), a new, one-dimensional,  
11 generic reactive-transport model (RTM) for the biogeochemical dynamics of carbon and  
12 associated bio-elements (*N*, *P*, *Si*) in estuaries. RTMs are well-established quantitative tools to  
13 disentangle the complex biogeochemical dynamics of estuaries (Thouvenin et al., 1994;  
14 **Regnier et al., 1997**; Regnier et al., 2003; Arndt et al., 2007; Vanderborgh et al., **2002**, 2007;  
15 Arndt et al., 2009), including their response to anthropogenic perturbations (Paerl et al., 2006;  
16 Thieu et al., 2010) and the complex process interplay that underlies system-wide key  
17 biogeochemical indicators, such as Net Ecosystem Metabolism (NEM), an integrative  
18 measure of the whole system biogeochemical dynamics defined as the difference between Net  
19 Primary Production (NPP), aerobic degradation and denitrification on a system scale (Odum,  
20 1956; Andersson and Mackenzie, 2004). C-GEM is not only computationally efficient, but  
21 also reduces data-requirements by using an idealized representation of the estuarine geometry  
22 to support hydrodynamic calculations and, subsequently, transport and biogeochemical  
23 reaction processes. The C-GEM modelling platform is **thus** compatible with hundreds to  
24 thousands of stationary or fully transient simulations (including daily to seasonal fluctuations)  
25 on a time span of years to decades, using geometric information readily available through

1 maps or remote sensing images. Moreover, unlike simpler box model approaches, which are  
2 still widely used to assess global estuarine dynamics (e.g. Andersson et al., 2005; Slomp and  
3 Van Cappellen, 2007; Laruelle, 2009; Mackenzie et al., 2012), C-GEM resolves the most  
4 important temporal and spatial scales and provides an accurate description of the estuarine  
5 hydrodynamics and transport. It may thus represent a promising avenue towards the  
6 development of a generalized method for exploring and quantifying biogeochemical  
7 transformations and fluxes in alluvial estuaries at the regional and/or global scale.

8 In the first part of this paper, the general structure of C-GEM is described. This includes  
9 detailed descriptions of the model support, of the fundamental equations for the  
10 hydrodynamics and transport and their parameterization and of the biogeochemical reaction  
11 network. In addition, a generic protocol for the set-up of C-GEM for an estuarine system is  
12 illustrated and different strategies will be proposed depending on the availability of data to  
13 constrain model parameters. The second part of this paper presents, as a proof of concept, the  
14 application of C-GEM to the funnel-shaped Scheldt estuary (Belgium-The Netherlands). The  
15 macro-tidal Scheldt estuary is among the best-surveyed estuarine systems worldwide and has  
16 been the subject of intense modeling efforts (e.g. Wollast and Peters, 1978; Soetaert and  
17 Herman, 1995; Regnier et al., 1997; Vanderborgh et al., 2002, 2007; Billen et al., 2005;  
18 Desmit et al., 2005; Hofmann et al., 2008; Arndt et al., 2009, 2011; Gypens et al., 2013). In  
19 order to test the performance of C-GEM in predicting the estuarine hydrodynamics and  
20 biogeochemical dynamics, both steady-state simulations for average summer conditions, as  
21 well as transient simulations for an entire year (2003) are carried out. Steady-state simulations  
22 are compared with a comprehensive set of field observations, while mass budget results, as  
23 well as NEM, derived from the transient simulation, are compared with results from a highly  
24 resolved 2D-RTM for the same period (Arndt et al., 2009). This model-data, model-model  
25 comparison allows assessing the model's performance on different temporal and spatial

1 scales. In addition, a sensitivity analysis is carried out to identify model parameters that exert  
2 the most important control on biogeochemical processes and to assess the sensitivity of  
3 estimated process rates to uncertainties in these parameter values. Finally, current model  
4 limitations with respect to local, regional and, ultimately, global scale applications are  
5 critically analysed.

6

## 7 **2 The C-GEM platform**

### 8 **2.1 Model support**

9 Alluvial estuaries are commonly defined as systems that are characterized by a movable bed,  
10 consisting of sediments of both marine and terrestrial origin, and a measurable influence of  
11 freshwater discharge (Savenije, 2005, 2012). In such estuaries, the amount of water flow  
12 entering or leaving the estuarine channel is entirely controlled by the shape of the estuary  
13 (Pethick, 1984). In turn, the water movement, driven by tides and freshwater discharge, leads  
14 to a redistribution of the unconsolidated sediments and determines the shape of the estuary.  
15 Alluvial estuaries display a wide variety of shapes ranging from funnel-shaped estuaries with  
16 a dominant tidal influence to prismatic estuaries with a large fluvial influence. Nevertheless,  
17 they bear common geometric characteristics that are compatible with an idealized  
18 representation of an estuary (Savenije, 1992, 2005, 2012). For tidally-averaged conditions,  
19 their cross-sectional area  $\bar{A}$  or width  $\bar{B}$  can be described by decreasing exponential functions  
20 with distance,  $x$ , from the mouth (Savenije, 1986, 2005, 2012):

$$21 \quad \bar{A} = A_0 \cdot \exp\left(-\frac{x}{a}\right) \quad (1)$$

$$22 \quad \bar{B} = B_0 \cdot \exp\left(-\frac{x}{b}\right) \quad (2)$$

1 where  $A_0$  and  $B_0$  are the cross-sectional area and the width at the estuarine mouth ( $x=0$ ),  
2 respectively,  $a$  is the cross-sectional convergence length and  $b$  is the width convergence  
3 length. Combining Eqs. (1) and (2) leads to an expression for the mean longitudinal variation  
4 in estuarine depth,  $h$  (Savenije, 2005):

$$5 \quad h = \frac{A_0}{B_0} \exp\left(-\frac{x(a-b)}{ab}\right) \quad (3)$$

6 Savenije (1992) showed that alluvial estuaries can be classified according to the Canter-  
7 Cremers number,  $N$ , and the estuarine shape-number,  $S$ . The dimensionless hydrodynamic  
8 Canter-Cremers number for flood discharge is defined as the ratio between the volume of the  
9 river discharge and the volume of saline water flowing into the estuary during a tidal period  
10 (Savenije, 2012):

$$11 \quad N = \frac{Q_b \cdot T}{P} \quad (4)$$

12 where  $Q_b$  is the bankfull discharge, defined as the momentary maximum flow, which has an  
13 average recurrence interval of 1.5 years, associated to a state of maximum velocity in the  
14 channel and, therefore, to the maximum ability to govern the shape and the size of the  
15 channel.  $T$  is the tidal period, which corresponds to the interval between successive high (or  
16 low) tides, and  $P$  is the tidal prism that represents the amount of water that flows in and out an  
17 estuary between high and low tide. The dimensionless estuarine shape number is a geometric  
18 parameter defined as the ratio between the convergence length  $a$  and the tidally-averaged  
19 depth at the estuarine mouth ( $h_0$ ):

$$20 \quad S = \frac{a}{h_0} \quad (5)$$

1 These two numbers provide a theoretical framework to analyse the tight link between the  
2 geometry and hydrodynamics of estuaries (Fig. 1). We can see that estuaries with a large  $Q_b$   
3 are more riverine and have a long convergence length. On the other hand, estuaries with a  
4 large tidal prism are generally deep and have a short convergence length. Based on Fig. 1,  
5 three main types of alluvial estuaries can be distinguished. Small  $N$  ( $<0.01$ ) and  $S$  ( $<8000$ )  
6 values characterize **tidally-dominated** funnel-shaped estuaries, while **fluvial-dominated**  
7 prismatic estuaries display high  $N$  ( $>15$ ) and  $S$  ( $>15000$ ) and mixed-type estuaries fall in  
8 between these two end-member cases. For instance, **estuaries such as** the Limpopo estuary  
9 (Fig. 2a) **have** a long convergence length **and a dominant fluvial influence** and **show** a  
10 longitudinal salt intrusion distribution that exponentially declines towards the land. At the  
11 opposite end of the shape spectrum, the Scheldt estuary has a short convergence length and a  
12 marine character, with a dome-shaped salt intrusion curve (Fig. 2c). The Incomati estuary is a  
13 good representation of the mixed category, showing a **half-gaussian** shaped salt intrusion  
14 curve (Fig. 2b).

15 The recognition of this tight link between estuarine geometry, hydrodynamics and transport  
16 (Fig. 2) and the identification of three main estuarine types (Fig. 1) becomes important when  
17 thinking about estuarine biogeochemical dynamics and its significance for global  
18 biogeochemical cycles. Because estuarine hydrodynamics exert a first order control on  
19 transport and biogeochemical processes (Fig. 3), estuarine biogeochemical characteristics,  
20 such as NEM, carbon and nutrient filtering capacities or  $\text{CO}_2$  exchange fluxes can potentially  
21 be directly linked to hydrodynamic and, thus geometrical characteristics. Such direct  
22 relationships between biogeochemical and readily available geometric characteristics would  
23 not only serve as a promising basis for a biogeochemical classification scheme, but would  
24 also significantly facilitate a quantitative assessment of the role of estuaries in global

1 biogeochemical cycles and its response to anthropogenic perturbations including land-use and  
2 climate change (Regnier et al., 2013b).

### 3 **2.2 Hydrodynamics**

4 Estuaries are subject to tidal forcing and freshwater inflow. At the estuarine mouth, tidal  
5 variations in water level induce a tidal wave. This wave travels upstream and is progressively  
6 distorted due to the combined influence of the estuarine geometry and river discharge. The  
7 tidal range is, to a first order, determined by the balance between energy gain through channel  
8 convergence and energy loss through friction on the estuarine bed. As a result, fundamental  
9 hydrodynamic characteristics, such as tidal range, tidal excursion and the phase lag of the  
10 tidal wave vary along the estuarine gradient and can be related to key geometric  
11 characteristics, such as convergence lengths or depth.

12 For weakly stratified or well-mixed estuaries whose depth is much smaller than width, the  
13 hydrodynamics can be described by the one-dimensional barotropic, cross-sectionally  
14 integrated mass and momentum conservation equations for a channel with arbitrary geometry  
15 (Nihoul and Ronday, 1976; Regnier et al., 1998; Regnier and Steefel, 1999):

16 
$$r_s \frac{\partial A}{\partial t} + \frac{\partial Q}{\partial x} = 0 \quad (6)$$

17 
$$\frac{\partial U}{\partial t} + U \frac{\partial U}{\partial x} = -g \frac{\partial \zeta}{\partial x} - g \frac{U|U|}{C^2 H} \quad (7)$$

18 where:

19  $t$  time [s]

20  $x$  distance along the longitudinal axis [m]

21  $A$  cross-section area  $A = H \cdot \bar{B}$  [m<sup>2</sup>]

1	$Q$	cross-sectional discharge $Q = A \cdot U$	$[\text{m}^3 \text{s}^{-1}]$
2	$U$	flow velocity	$[\text{m}^2 \text{s}^{-1}]$
3	$r_s$	storage ratio $r_s = B_s / \bar{B}$	[-]
4	$B_s$	storage width	[m]
5	$g$	gravitational acceleration	$[\text{m s}^{-2}]$
6	$\zeta$	elevation	[m]
7	$C$	Chézy coefficient	$[\text{m}^{1/2} \text{s}^{-1}]$
8	$H$	water depth $H = h + \zeta(x, t)$	[m]

9 The coupled partial differential equations (Eqs. (6) and (7)) are solved by specifying the  
10 elevation  $\zeta_0$  at the estuarine mouth and the river discharge  $Q_r(t)$  at the upstream limit of the  
11 model domain.

12 Bed friction exerted on the moving water is described by means of a roughness formulation  
13 following Manning-Strickler (Savenije, 2012):

$$14 \quad C = \frac{1}{n} H^{1/6} \quad (8)$$

15 where  $C$  is the Chézy coefficient,  $n$  is the channel roughness coefficient or the dimensionless  
16 Manning's number and  $H$  is the water depth. The bed roughness, which depends on the  
17 bottom material and on the depth of the flow, is a notoriously difficult parameter to measure  
18 and is generally constrained via model calibration by fitting simulated water elevations, tidal  
19 wave propagation and current velocities to observations. In the absence of data, a realistic  
20 mean range for  $C$  is comprised between 40 and 60  $\text{m}^{1/2} \text{s}^{-1}$  (Savenije, 2001, 2012). Lower

1 values can typically be applied in the shallow tidal river where bottom friction is significant,  
2 while higher values can be applied in the saline estuary.

### 3 **2.3 Mass conservation for solutes**

4 The one-dimensional, tidally-resolved, advection-dispersion equation for a solute  $C(x,t)$  in an  
5 estuary can be written as (e.g. Pritchard, 1958):

$$6 \quad \frac{\partial C}{\partial t} + \frac{Q}{A} \frac{\partial C}{\partial x} = \frac{1}{A} \frac{\partial}{\partial x} \left( AD \frac{\partial C}{\partial x} \right) + P \quad (9)$$

7 In Eq. (9),  $Q$  and  $A$  are provided by the hydrodynamic model and  $P$  is the sum of all  
8 production and consumption process rates for the solute  $C$ . The effective dispersion  
9 coefficient  $D$  ( $\text{m}^2 \text{s}^{-1}$ ) implicitly accounts for dispersion mechanisms associated to sub-grid  
10 scale processes (Fischer, 1976; Regnier et al., 1998). In general,  $D$  is maximal near the sea,  
11 decreases upstream and becomes virtually zero near the tail of the salt intrusion curve  
12 (Preddy, 1954; Kent, 1958; Ippen and Harleman, 1961; Stigter and Siemons, 1967). The  
13 effective dispersion at the estuarine mouth can be quantified by the following relation (Van  
14 der Burgh, 1972):

$$15 \quad D_0 = 26 \cdot (h_0)^{1.5} \cdot (N \cdot g)^{0.5} \quad (10)$$

16 where  $h_0$  (m) is the tidally-averaged depth at the estuarine mouth,  $N$  is the dimensionless  
17 Canter Cremers' estuary number defined as the ratio of the freshwater entering the estuary  
18 during a tidal cycle to the volume of salt water entering the estuary over a tidal cycle (Eq. (4))  
19 and  $g$  ( $\text{m s}^{-2}$ ) is the gravitational acceleration. The variation in  $D$  along the estuarine gradient  
20 can be described by Van der Burgh's equation (Savenije, 1986):

$$21 \quad \frac{\partial D}{\partial x} = -K \frac{Q_r}{A} \quad (11)$$

1 where  $K$  is the dimensionless Van der Burgh's coefficient and the minus sign indicates that  $D$   
2 increases in downstream direction (Savenije, 2012). The Van der Burgh's coefficient is a  
3 shape factor that can be shown to have values between 0 and 1 (Savenije, 2012), which  
4 depends on geometry and tidally average conditions. Therefore, each estuarine system has its  
5 own characteristic  $K$  value, which correlates with geometric and hydraulic scales (Savenije,  
6 2005). It has thus been proposed, based on a regression analysis covering a set of 15 estuaries,  
7 that  $K$  can be constrained from the estuarine geometry (Savenije, 1992):

$$8 \quad K = 4.32 \cdot \frac{h_0^{0.36}}{B_0^{0.21} \cdot b^{0.14}} \quad \text{with} \quad 0 < K < 1 \quad (12)$$

## 9 **2.4 Biogeochemical reactions**

10 The reaction network for the water column estuarine biogeochemistry includes total  
11 (particulate and dissolved) organic carbon ( $TOC$ ), oxygen ( $O_2$ ), ammonium ( $NH_4$ ), nitrate  
12 ( $NO_3$ ), phosphate ( $PO_4$ ), dissolved silica ( $dSi$ ) and phytoplankton biomass ( $PHY$ ) as state  
13 variables. The reaction network considers the essential biogeochemical processes that affect  
14 carbon and associated bio-elements: primary production, phytoplankton mortality, aerobic  
15 degradation, denitrification, nitrification and  $O_2$  exchange across the air-water interface.  
16 Variables and process rates included in C-GEM are schematized in Fig. 4 and their  
17 formulations and stoichiometric equations are summarized in Table 1.

18 Despite its limited set of reaction processes, the simplicity of the biogeochemical network  
19 warrants application in data-poor systems. The gross primary production rate,  $GPP$ , is  
20 controlled by the underwater light regime that explicitly accounts for the effect of the  
21 suspended particulate matter (see below) and neglects phytoplankton self-shadowing, an  
22 effect that is generally weak in turbid estuarine systems (Desmit et al., 2005). In addition,  
23 macronutrient concentrations ( $dSi$ ,  $DIN=NO_3+NH_4$  and  $PO_4$ ) limit phytoplankton growth

1 through a succession of Michaelis-Menten terms, each with their corresponding half-  
2 saturation constant,  $K_{MM}$ . Net primary production,  $NPP$ , is calculated as the difference  
3 between  $GPP$  and autotrophic phytoplankton respiration, which accounts for biosynthesis,  
4 maintenance and excretion. Biosynthesis and excretion terms are assumed to be linearly  
5 proportional to  $GPP$  (Weger et al., 1989; Langdon, 1993; Lancelot et al., 2000), while the  
6 maintenance term is a direct function of the total phytoplankton concentration (Vanderborcht  
7 et al., 2002). The gradual switch between ammonium and nitrate utilization pathways for  $NPP$   
8 is controlled by the availability of ammonium. Phytoplankton mortality is linearly  
9 proportional to the phytoplankton concentration through a mortality rate constant,  $k_{mort}$ , which  
10 integrates the combined effects of cell lysis and grazing by higher trophic level. Upon death,  
11 phytoplankton contributes to the total organic matter pool. **The latter is represented as a single  
12 pool including only the fraction of the organic carbon, which actively contributes to the short-  
13 term supply of inorganic nutrients (Regnier and Steefel, 1999). Thus, the model does not  
14 account for burial of (refractory) particulate organic carbon in estuarine sediments (Abril et  
15 al., 2002; Vanderborcht et al., 2007).** Organic matter is degraded by aerobic degradation,  
16  $aer\_deg$ , and denitrification,  $denit$ . If oxygen concentrations are sufficient,  $aer\_deg$  is the  
17 most energetically favourable pathway and, thus, dominates the other metabolic processes  
18 (e.g. Stumm and Morgan, 1996).  $denit$  becomes important in polluted estuaries where oxygen  
19 levels drop to limiting concentrations. The heterotrophic degradation processes are described  
20 by a Michaelis-Menten terms for both organic carbon and electron acceptor concentration  
21 (Regnier et al., 1997). By oxidizing  $NH_4$  to  $NO_3$ , nitrification,  $nit$ , consumes large amounts of  
22  $O_2$  in polluted estuaries (Soetaert and Herman, 1995; Regnier and Steefel, 1999; Andersson et  
23 al., 2006; Hofmann et al., 2008). It is formulated as a one-step process including two  
24 Michaelis-Menten terms with respect to  $O_2$  and  $NH_4$ . The temperature dependence of  
25 maximum degradation rates,  $k_{ox}$  and  $k_{denit}$ , and maximum nitrification rate,  $k_{nit}$ , is expressed

1 via a function with a  $Q_{10}$  value. Oxygen transfer through the air-water interface,  $O_{2,ex}$ , exerts  
 2 an important influence on the oxygen concentration in the water column. The exchange rate is  
 3 expressed by the product of a piston velocity ( $vp$ ) and the difference between oxygen  
 4 concentration and oxygen saturation. The latter is calculated as a function of temperature and  
 5 salinity (Benson and Krause, 1984), while the piston velocity is calculated as the sum of two  
 6 terms attributed to the current velocity and the wind speed at 10 m above the air-water  
 7 interface (Regnier et al., 2002). At this stage, the benthic-pelagic exchange is not included in  
 8 the model, although cost-efficient numerical approaches are available for carbon and nutrients  
 9 (e.g. Jahnke et al., 1982; Ruardij and van Raaphorst, 1995; Soetaert et al., 1996; Arndt and  
 10 Regnier, 2007; Gypens et al., 2008). Hence, the application of C-GEM to shallow, pristine  
 11 estuarine systems subject to intense element recycling within the sediments is not  
 12 recommended at this stage.

## 13 **2.5 Suspended particulate matter**

14 The simulation of the suspended particulate matter (SPM) dynamics is required for the  
 15 prediction of the light availability within the water column that exerts an important control on  
 16 primary production in turbid estuaries, mainly. The one-dimensional, tidally-resolved,  
 17 advection-dispersion equation for suspended particulate matter (SPM) dynamics follows an  
 18 equation similar to that of solutes (Eq. (9)) with the addition of two extra terms describing the  
 19 mass exchange with the material surfaces of the estuarine bed:

$$20 \quad \frac{\partial SPM}{\partial t} + \frac{Q}{A} \frac{\partial SPM}{\partial x} = \frac{1}{A} \frac{\partial}{\partial x} \left( AD \frac{\partial SPM}{\partial t} \right) + (R_{ero} - R_{dep}) \quad (13)$$

21 where  $R_{ero}$  and  $R_{dep}$  denote the erosion and deposition rates, respectively. In the theory of  
 22 cohesive sediment transport, they are often considered to be mutually exclusive (Sanford and

1 Halka, 1993) and expressed according to the well-established formulation of Partheniades  
 2 (1962) and Einstein and Krone (1962):

$$3 \quad R_{ero} = \frac{1}{H} \cdot p_{ero} \cdot E \quad (14)$$

$$4 \quad R_{dep} = \frac{1}{H} \cdot p_{dep} \cdot w_s \cdot SPM \quad (15)$$

5 where  $H$  denotes the water depth and  $p_{ero}$  and  $p_{dep}$  (-) are the probabilities for erosion and  
 6 deposition, respectively.  $E$  ( $\text{mg m}^{-2} \text{s}^{-1}$ ) is the erosion coefficient, while  $w_s$  ( $\text{m s}^{-1}$ ) is the  
 7 settling velocity of particles.  $p_{ero}$  and  $p_{dep}$  are given by (Einstein and Krone, 1962; Dyer, 1986;  
 8 Mehta et al., 1989):

$$9 \quad p_{ero} = \begin{cases} \frac{\tau_b}{\tau_{cr}} - 1 & \tau_{cr} \leq \tau_b \\ \tau_{cr} & \tau_{cr} > \tau_b \\ 0 & \tau_{cr} > \tau_b \end{cases} \quad (16)$$

$$10 \quad p_{dep} = \begin{cases} 1 - \frac{\tau_b}{\tau_{cr}} & \tau_{cr} \geq \tau_b \\ \tau_{cr} & \tau_{cr} > \tau_b \\ 0 & \tau_{cr} > \tau_b \end{cases} \quad (17)$$

11 where  $\tau_{cr}$  ( $\text{N m}^{-2}$ ) is the critical shear stress for erosion and deposition. The bottom shear  
 12 stress,  $\tau_b$  ( $\text{N m}^{-2}$ ), is calculated dynamically using the quadratic friction law:

$$13 \quad \tau_b = \frac{\rho_w \cdot g \cdot |U| \cdot U}{C^2} \quad (18)$$

14 where  $\rho_w$  ( $\text{kg m}^{-3}$ ) is the pure water density.

15 All SPM parameters ( $\tau_{cr}$ ,  $\tau_b$ ,  $E$ ,  $w_s$ ) implicitly account for geomorphological and biological  
 16 processes, such as sediment composition or biological stabilization mechanisms that are not  
 17 explicitly resolved (e.g. Wolanski et al., 1992; Cancino and Neves, 1999; van Ledden et al.,

1 2004). SPM parameter values are generally derived by model calibration against locally  
2 observed SPM data and their transferability to other estuarine systems may thus be limited.

### 3 **2.6 Numerical Solution**

4 The non-linear partial differential equations are solved by a finite difference scheme on a  
5 regular grid, with a grid size  $\Delta x=2000\text{m}$  and using a time step  $\Delta t=150\text{s}$ . If required, both  
6 spatial and temporal resolution can easily be modified. Transport and reaction terms are  
7 solved in sequence within a single timestep using an operator splitting approach (Regnier et  
8 al., 1997). The advective term in the transport equation is integrated using a third-order  
9 accurate total variation diminishing algorithm with flux limiters, ensuring monotonicity  
10 (Leonard, 1984), while a semi-implicit Crank-Nicholson algorithm is used for the dispersive  
11 term (Press et al., 1992). The schemes have been extensively tested using the CONTRASTE  
12 estuarine model (e.g. Regnier et al., 1998; Regnier and Steefel, 1999; Vanderborgh et al.,  
13 2002) and guarantee mass conservation to within  $<1\%$ . The erosion-deposition terms, as well  
14 as the reaction network, are numerically integrated using the Euler method (Press et al.,  
15 1992). The Primary production dynamics, which requires vertical resolution of the photic  
16 depth, is calculated according to the method described in Vanderborgh et al. (2007).

17

## 18 **3 Protocol for the set-up of C-GEM**

19 The following section is a step-by-step protocol describing how to set-up C-GEM and  
20 specifying data requirements at each step. Each step of the set-up is described using direct  
21 references to the corresponding source code file of C-GEM provided as supplementary  
22 material (see section 7 at the end of the manuscript for more details).

### 23 **3.1 Step 1: Construction of the idealized geometry**

1 The idealized estuarine geometry is defined by the estuarine length ( $EL$ ) and the depth  
2 ( $DEPTH$ ), as well as the width ( $B$ ). The depth and the width are specified in *define.h* for both  
3 upper ( $B_{ub}$  and  $DEPTH_{ub}$ ) and lower ( $B_{lb}$  and  $DEPTH_{lb}$ ) boundaries. In general, and  
4 especially for navigable channels, estuarine bathymetric data are available or can be derived  
5 from navigation charts. If no data is available, the depth can be approximated using remote  
6 sensing data (Gao, 2009) or assumed to be about 7 m for alluvial estuaries (e.g. Savenije,  
7 1992). The estuarine width at both boundaries of the model domain can be easily derived  
8 from local maps. The width convergence length,  $LC$ , is then calculated in *init.c* using Eq. (2).  
9 The cross-sectional area is then calculated at every grid point by the product of water depth  
10 and estuarine width (see Eq. (6)).

## 11 **3.2 Step 2: Set-up of the hydrodynamic module**

### 12 *Step 2.1: Parameters*

13 The Chézy coefficient ( $Chezy$ ) is the only control parameter in the equation of motion. Its  
14 value is defined at the two boundaries of the model domain (*define.h*) and its variation in  
15 space is specified in *init.c*. The Chézy coefficient is rarely measured and, thus, generally  
16 calibrated (Savenije, 1992). If observations for model calibration are missing, typical values  
17 reported in the literature for alluvial estuaries are  $60 \text{ m}^{1/2} \text{ s}^{-1}$  in the saline zone and  $40 \text{ m}^{1/2} \text{ s}^{-1}$   
18 in the freshwater reaches (Savenije, 1992, 2001).

### 19 *Step 2.2: Boundary conditions*

20 The boundary conditions for the hydrodynamic module are specified in *define.h* and consist of  
21 the freshwater discharge ( $Q_r$ ) at the upstream boundary and the tidal elevation at the estuarine  
22 mouth, which requires specification of the amplitude ( $AMPL$ ) and the frequency ( $pfun$ ). Tidal  
23 elevation can be deduced from water level data obtained from gauging stations or estimated  
24 theoretically using an astronomical model (e.g. Regnier et al., 1998). The freshwater

1 discharge is often monitored in rivers, but when missing, it can be derived from local or  
2 global watersheds model outputs (Garnier et al., 2005; Fekete et al., 2002).

### 3 *Step 2.3: Validation*

4 Hydrodynamics can be validated by comparing simulated and observed tidal amplitude  
5 profiles. If water level time-series are not available, remote sensing data, such as laser  
6 altimetry, can be used to validate tidal wave amplitude and propagation (Cazenave and  
7 Savenije, 2008). Although promising, this method remains currently limited to a few locations  
8 (e.g. Syed et al., 2008).

## 9 **3.3 Step 3: Set-up of the salt transport module**

### 10 *Step 3.1: Parameters*

11 The dispersion coefficient at the estuarine mouth,  $D_0$ , and its longitudinal variation are the  
12 only controlling parameters of the transport module. They are calculated in *init.c*. according to  
13 Eqs. (10), (11) and (12).

### 14 *Step 3.2: Boundary conditions for salinity*

15 Boundary conditions for salinity are specified in *init.c*. In general, upper boundary condition  
16 is set to 0, while lower boundary condition can be extracted from local measurements or  
17 regional or global database, such as the World Ocean Atlas  
18 (<http://www.nodc.noaa.gov/OC5/indprod.html>).

### 19 *Step 3.3: Validation*

20 The validation of the transport module is typically performed by comparing simulated  
21 longitudinal salinity profiles with observed data collected along the estuarine gradient or by  
22 comparing simulated and measured time-series at given location (e.g. Regnier et al., 1998).  
23 Note that the transport module is based on a predictive model, which only requires

1 geometrical information. Hence, it can also be applied in estuaries for which salinity data are  
2 not available.

### 3 **3.4 Step 4: Set-up of the SPM module**

#### 4 *Step 4.1: Parameters*

5 The sediment settling velocity,  $w_s$ , the critical shear stress for erosion and deposition,  $\tau_{ero}$  and  
6  $\tau_{dep}$ , and the erosion coefficient,  $M_{ero}$ , are specified in *define.h*.  $\tau_{ero}$ ,  $\tau_{dep}$  and  $M_{ero}$  need to be  
7 defined at both upper and lower boundaries. If longitudinal variations in sediment parameters  
8 need to be implemented, their formulations are defined in *sed.c*. These parameters generally  
9 require calibration. However, since the bottom material of the wider part of alluvial estuaries  
10 consists of mud or fines sediments (Savenije, 1986),  $w_s$  rarely exceeds  $1 \text{ mm s}^{-1}$  (Winterwerp,  
11 2002). Other parameters, such as  $\tau_{ero}$ ,  $\tau_{dep}$  and  $M_{ero}$  are calibrated on the basis of observed  
12 SPM profiles. The latter is an important step where observations still remain essential.

#### 13 *Step 4.2: Boundary conditions*

14 Boundary conditions for SPM are specified in *init.c*. SPM concentrations are usually available  
15 for navigable channels, in particular those where dredging works are carried out. In case of  
16 data-poor systems, the upper boundary condition can be derived from global statistical  
17 models, such as GlobalNEWS2 (Mayorga et al., 2010). When no observations or models are  
18 available to constrain lower boundary conditions, SPM values can be deduced from remote  
19 sensing data (e.g. Bowers et al., 1998; Fettweis and Nechad, 2011).

#### 20 *Step 4.3: Validation*

21 SPM dynamics may be validated comparing simulated longitudinal profile along the estuarine  
22 axis and/or time-series modelled at given location with observed sediment concentrations.  
23 Otherwise, simulated concentrations can be validated using remote sensing and satellite data

1 (e.g. Stumpf, 1988; Moore et al., 1999; Robinson et al., 1999; Doxaran et al., 2002, 2009; van  
2 der Wal et al., 2010).

### 3 **3.5 Step 5: Set-up of the biogeochemical module**

#### 4 *Step 5.1: Definition of biogeochemical reaction network*

5 The C-GEM biogeochemical module is implemented in *biogeo.c* by defining all  
6 biogeochemical reaction equations and by implementing all stoichiometric coefficients for  
7 each variable of the model. This structure allows for a flexible implementation and a rapid  
8 extension of the network by, for instance, different phytoplankton groups or additional  
9 transformation processes, such as adsorption-desorption or benthic-pelagic exchange  
10 processes.

#### 11 *Step 5.2: Parameters*

12 All parameter values for the biogeochemistry are specified in *define.h*. In most estuaries,  
13 system-specific values for all required parameters are not available but a literature survey can  
14 provide reasonable ranges within which a calibration can be performed (e.g. Cerco and Cole,  
15 1994; Garnier et al., 1995; Le Pape et al., 1999; Desmit et al., 2005 for the phytoplankton  
16 mortality rate constant or Regnier et al., 1997, 1999; Park et al., 2005; Arndt et al., 2007,  
17 2009 and Vanderborcht et al., 2007 for the nitrification rate constant). Unfortunately,  
18 estuarine parameter values for the biogeochemistry remain to be assembled in a global  
19 database (Regnier et al., 2013b).

#### 20 *Step 5.3: Boundary conditions*

21 The boundary conditions required for the biogeochemical module are assigned a numerical  
22 value in *init.c*. If direct observations are not available, boundary conditions for the riverine  
23 inputs of organic carbon and nutrients can be extracted from the global watershed statistical

1 model GlobalNEWS2 (Mayorga et al., 2010), while boundary conditions at the downstream  
2 limit can be obtained from the World Ocean Atlas  
3 (<http://www.nodc.noaa.gov/OC5/indprod.html>).

#### 4 *Step 5.4: External forcings*

5 The biogeochemical module requires specification of a number of external forcings depending  
6 on the formulation used to describe biogeochemical processes. For instance, in this study,  
7 phytoplankton growth depends on irradiance, photoperiod and temperature. The latter also  
8 influences other biogeochemical transformations, such as heterotrophic degradation and  
9 nitrification, while wind speed is required to constrain the exchange rate at the air-water  
10 interface. In C-GEM, photoperiod, temperature and wind speed are specified in *define.h*,  
11 while irradiance is calculated in *fun.c*. All external forcings should preferably be derived from  
12 observations but, if direct observations are not available, irradiance and photoperiod can be  
13 constrain using radiation models (e.g. van der Goot, 1997) or may be extrapolated as a  
14 function of time, year and latitude using the astronomical equation of Brock (1981). Other  
15 external forcings can be obtained from global databases, such as the World Ocean Atlas  
16 (<http://www.nodc.noaa.gov/OC5/indprod.html>) for the water temperature and the CCMP  
17 dataset (Atlas et al., 2011) for the wind velocity.

### 18 **3.6 Step 6: Sensitivity analysis**

19 A sensitivity analysis is a crucial part of the iterative revision process of the model set-up.  
20 Depending on the results of each model validation and sensitivity analysis, the user may be  
21 required to repeat a step or even return to a previous step. The sensitivity analysis provides  
22 also useful information regarding the uncertainty in model predictions.

23

## 24 **4 Application to the funnel-shaped Scheldt Estuary: a test case**

## 1 **4.1 The Scheldt estuary**

2 The Scheldt river and its tributaries drain an area of 21580 km<sup>2</sup> in northern France, western  
3 Belgium and south-western Netherlands before discharging into the southern North Sea  
4 (Fig.5a). Its hydrographical basin includes one of the most populated regions of Europe,  
5 heavily affected by human activities (e.g. Wollast and Peters, 1978; Billen et al., 1985;  
6 Soetaert et al., 2006). The part of the river that is influenced by the tide is referred as the  
7 Scheldt estuary extending 160 km from the estuarine mouth at Vlissingen (Netherlands) to  
8 Gent (Belgium), where a sluice blocks the tidal wave. The tide is semi-diurnal with an  
9 amplitude of about 4 m (Regnier et al., 1998). Salt intrudes as far as 100 km from the  
10 estuarine mouth. Upstream of km 100, the estuary is characterized by a complex network of 6  
11 tributaries (Dender, Durme, Grote Nete, Kleine Nete, Zenne and Dijle). The latter four form  
12 the Rupel, a single stream, which rejoins the main channel of the Scheldt at the salt intrusion  
13 limit.

## 14 **4.2 Model set-up**

### 15 **4.2.1 Geometry**

16 The Scheldt estuary is characterized by a large tidal range inducing a short convergence  
17 length (Table 2) and can be thus classified as a funnel-shaped system (Fig. 1) (Savenije,  
18 2005). Figure 5 compares the geometry of the Scheldt (Fig. 5a) to its idealized geometry  
19 (Figs. 5b and 5c) derived from the width convergence length, water depth and tidal amplitude.  
20 A variable depth ( $h$ ) is applied here to account for a small, constant bottom slope over the  
21 total estuarine length. This idealized geometry (Figs. 5b and 5c) forms the support for C-GEM  
22 and illustrates the typical features of a funnel-shaped estuary: wide and deep at the mouth  
23 with a short convergence length, which induces a rapid upstream decrease in width.

### 24 **4.2.2 Boundary conditions**

1 Both steady-state and transient model simulations are conducted to test the performance of C-  
2 GEM. For both cases, a spin-up period of two months is imposed. In addition, a constant tidal  
3 amplitude is applied at the estuarine mouth. The tidal amplitude only accounts for the  
4 dominant semi-diurnal component M2, characterized by a period of 12.42 hr and a frequency  
5 of 0.080 cycles/hours (Regnier et al., 1998).

6 For the steady-state simulations, a constant river discharge is specified at the inland limit of  
7 the Scheldt and its tributaries. In addition, constant biogeochemical boundary conditions and  
8 physical forcings (e.g. temperature and light intensity), representative for the summer  
9 conditions during the 1990's (Table 3; for further details see Vanderborcht et al., 2007), are  
10 applied. To validate C-GEM, simulation results are then compared to observations extracted  
11 from the OMES database (Maris et al., 2004; Vanderborcht et al., 2007) for similar  
12 conditions.

13 Fully-transient simulations using daily, weekly or monthly transient boundary conditions and  
14 external forcings for the year 2003 (see Arndt et al., 2009 for details) are performed to test the  
15 performance of C-GEM in quantifying integrative, system-scale biogeochemical indicators,  
16 such as NEM. These integrative indicators cannot be easily quantified on the basis of  
17 observations alone and its quantitative assessment, thus, requires the application of model  
18 approaches (e.g. Arndt et al., 2009, 2011; Regnier et al., 2013b). Here, C-GEM results are  
19 compared to the outputs from a carefully calibrated and validated, highly-resolved horizontal  
20 2D reactive transport model (Arndt et al., 2009). The latter uses a total of 56000  
21 computational points and provides a very detailed representation of the estuarine morphology.  
22 Both models are forced with identical boundary conditions and physical forcings (see Arndt et  
23 al., 2009 for a detailed description).

#### 24 **4.2.3 Suspended Particulate Matter and Biogeochemistry**

1 For the sake of comparison, all biogeochemical parameters and the biogeochemical reaction  
2 network, described in section 2.4, are identical to those used in Arndt et al. (2009), with the  
3 exception of the Michaelis-Menten constant for phosphate ( $K_{PO_4}$ ), a variable not included in  
4 Arndt et al. (2009), and the maximum specific photosynthetic rate ( $P_{max}^B$ ), which is constant in  
5 the stationary simulation and varies with temperature in the transient simulation (see Table 1).  
6 A complete list of biogeochemical parameters is presented in Table 4. In the Scheldt estuary,  
7 diatoms are the dominant phytoplankton species (e.g. Mulyaert and Sabbe, 1999). Hence,  
8 *GPP* is assumed to be carried out by diatoms only ( $PHY=DIA$ ). Because of the **large**  
9 **anthropogenic influence on** the Scheldt estuary, **which favours net heterotrophy**, nitrogen and  
10 phosphorous levels are typically well above limiting concentrations (Meire et al., 2005; Van  
11 Damme et al., 2005; Soetaert et al., 2006; Vanderborght et al., 2007) and silica can be  
12 assumed as the only limiting nutrient for diatom growth (Arndt et al., 2007). Sediment  
13 parameters are calibrated on the basis of SPM observations and by comparing the simulated  
14 annual evolution of NPP and sediment concentration with results obtained from the 2D  
15 model. SPM parameter values are provided in Table 5.

#### 16 **4.2.4 Lateral loads and Rupel's network**

17 Lateral inputs from domestic, industrial and agricultural activities are accounted in the model  
18 and are applied in all runs as constant point sources of organic matter, ammonium and nitrate  
19 distributed along the estuarine gradient (Vanderborght et al., 2007; Arndt et al., 2009). Their  
20 values and their input locations are given in Table 6. Differences between lateral loads use for  
21 stationary and transient simulations mainly reflect the improvement of wastewater treatment  
22 in the Scheldt catchment at the end of the 20th century (Vanderborght et al., 2007).

23 In addition, C-GEM also accounts for the river network of the Rupel, the most important  
24 tributary of the Scheldt (Hellings and Dehairs, 2001) in form of a simple box model with a

1 volume of about  $1.5 \cdot 10^7 \text{ m}^3$  that discharges unilaterally in the main channel at km 102 (Figs.  
2 5b and 5c). This approach allows for a better comparison between simulation results and field  
3 data. Rupel's boundary conditions are listed in Table 3.

#### 4 **4.3 Sensitivity Study**

5 A sensitivity analysis, using a one factor at a time (OFAT) method, was conducted to assess  
6 the influence of model parameter variations on Net Primary Production (NPP), aerobic  
7 degradation (R), denitrification (D), nitrification (N),  $O_2$  exchange across air/water interface  
8 ( $O_2\text{ex}$ ) and Net Ecosystem Metabolism (NEM). The original parameter set adopted by the 2D  
9 model (Arndt et al., 2009) serves as a reference case for the sensitivity study. The sensitivity  
10 of spatially and temporally integrated rates to parameter changes is investigated. Table 7  
11 provides an overview of the model parameters, their baseline values, as well as the tested  
12 parameter range. Note that the Chézy coefficient is considered as a sediment parameter  
13 despite its dual role on hydrodynamics and sediment erosion/deposition dynamics (see Eqs.  
14 (7) and (18)). **Although sediment and biogeochemical parameters, such as for instance the rate**  
15 **constant of organic matter degradation (e.g. Arndt et al., 2013), can vary over orders of**  
16 **magnitude, here they** are varied arbitrarily over a range of  $\pm 50\%$  of their baseline value  
17 **because our** aim is to test the relative sensitivity of the model response and establish priorities  
18 for future research rather than to assess the variability arising from different ranges in  
19 parameter values reported in literature. On the other hand, geometric parameters (convergence  
20 length and depth) are varied over a smaller range ( $\pm 10\%$  and  $\pm 20\%$ , respectively) since they  
21 can be constrained on the basis of observations.

#### 22 **4.4 From hydrodynamics to biogeochemistry**

##### 23 **4.4.1 Hydrodynamics and Transport**

1 The simulated longitudinal profile of the tidal amplitude (Fig. 6) reveals the characteristic  
2 features of a funnel-shaped, macro-tidal estuary (Savenije and Veling, 2005; Arndt et al.,  
3 2007; Nguyen, 2008). In the lower, tidally-dominated part of the estuary, channel  
4 convergence results in the amplification of the tidal wave. However, the influence of fluvial  
5 energy progressively increases as the tidal wave moves upstream. It acts primarily through  
6 bottom friction and induces a dampening of the tidal amplitude (Fig. 6). High water levels are  
7 less influenced by friction than low water levels and thus contribute less to the decrease in  
8 tidal range. Figure 6 shows that the model slightly underestimates the tidal amplitude in the  
9 saline estuary ( $km < 100$ ), while it overestimates the tidal amplitude in the tidal river. In  
10 particular, mean relative differences between observed and simulated tidal amplitudes are  
11 smaller than 5% and 22% in the saline estuary and in tidal river, respectively. Discrepancies  
12 between model results and observations are mainly related to the seasonal and inter-annual  
13 variability in freshwater discharge, which cannot be captured by the steady-state simulation.  
14 Part of the deviation may also arise from the use of an idealized geometry, which does not  
15 resolve the complex bathymetry of the Scheldt estuary that is characterized by deep tidal  
16 channels and shallow tidal flats.

17 The dispersion coefficient  $D$  is quantified according to Eq. (11) using the idealized geometry  
18 of the Scheldt (shown in Figs. 5b and 5c and summarized in Table 2) and assuming constant  
19 freshwater discharge of  $39 \text{ m}^3 \text{ s}^{-1}$  corresponding to the mean value for which observations  
20 were available. These assumptions yield a Van der Burgh's coefficient  $K$  of 0.39. Figure 7  
21 illustrates the evolution of the dispersion coefficient  $D$  along the estuarine gradient and  
22 reveals a dome-shaped profile with a maximum value of about  $124 \text{ m}^2 \text{ s}^{-1}$  near the estuarine  
23 mouth that reduces to 0 in the tidal river.

1 The longitudinal distribution of salinity is controlled by the balance between upstream  
2 dispersion and downstream advection (Savenije, 2005, 2012). The steady-state salinity profile  
3 (Fig. 8) also follows a dome-shaped distribution characterized by a small salinity gradient at  
4 the estuarine mouth. This shape is typical of funnel-shaped estuaries (e.g. Savenije, 2005).  
5 Simulation results (Fig. 8) agree well with salinity distributions observed under similar  
6 hydrodynamic conditions (Regnier et al., 1998).

#### 7 **4.4.2 SPM and Biogeochemistry**

8 The estuarine SPM distribution is mainly controlled by the total dissipation of tidal and fluvial  
9 energies (Chen, 2003; Chen et al., 2005; Arndt et al., 2007). **Although SPM concentrations in**  
10 **the Scheldt estuary show a very patchy pattern in time and space due to their high sensitivity**  
11 **to changes in physical forcing conditions (Van Damme et al., 2005), a typical trend, which**  
12 **relates to three well-defined energy regimes along the longitudinal axis of the estuary, can be**  
13 **identified** (e.g. Jay et al., 1990; Dalrymple et al., 1992; Arndt et al., 2007). In the lower  
14 estuary, **where** mechanical energy is almost exclusively provided by the tide, **observed SPM**  
15 **concentrations are generally low and range between 0 and 150 mg l<sup>-1</sup> (Van Damme et al.,**  
16 **2005). Moving upstream, channel convergence induces an upstream increase in energy**  
17 **dissipation and the associated intensification** in tidal amplitude (e.g. Fig. 6) triggers an  
18 increase in SPM concentrations from the mouth to the turbidity maximum zone (TMZ), where  
19 maximum value of up to 600 mg l<sup>-1</sup> can be observed (Van Damme et al., 2005). The exact  
20 location of the TMZ shifts in response to the tidal excursion and the river discharge and is  
21 generally found between km 60 and km 100 (e.g. Wollast and Marijns, 1981; Chen et al.,  
22 2005). **Beyond** of the TMZ, friction progressively reduces the tidal influence (Horrevoets et  
23 al., 2004) and energy dissipation becomes progressively controlled by the seaward flux of  
24 fluvial energy. **At the** so-called balance point, where both contributions are of similar but low

1 magnitude, low SPM concentrations are observed (0-250 mg l<sup>-1</sup>, Van Damme et al., 2005).  
2 Upstream of the balance point, close to the estuarine upper limit, the magnitude of the riverine  
3 input flux controls the SPM concentration (Chen et al., 2005). The simulated steady-state  
4 longitudinal SPM profile (Fig. 9) is in agreement with this general pattern. Direct comparison  
5 with an observed SPM profile is however not possible because the simulated steady-state  
6 conditions do not reproduce a situation observed in the field. SPM concentrations are strongly  
7 controlled by local exchange processes with the estuarine bed. Hence, already small changes  
8 in the physical forcing, as well as their history, exert a large impact on local SPM  
9 concentrations and result in large local fluctuation, rendering a direct comparison of  
10 simulation results and the range of observed SPM values little informative.

11 Longitudinal steady-state profiles of oxygen, ammonium, nitrate and silica generally show a  
12 good agreement with measured data (Fig. 10). These profiles are discussed in details in  
13 Vanderborgh et al. (2007) and some key features are briefly summarized here. In the tidal  
14 river, high riverine loads of carbon and reduced nitrogen drive intense heterotrophic processes  
15 rates and, thus, trigger low oxygen concentrations (Fig. 10a). Further downstream, the  
16 decrease in consumption rates and the increase in air-water exchange fluxes results in a  
17 progressive increase in  $O_2$  levels. In contrast, nutrient concentrations are generally high in the  
18 upper tidal reaches, but decrease along the estuarine gradient due to the progressive dilution  
19 and the decrease in autotrophic process rates (Figs. 10b-d). A short increase in  $NH_4$  (Fig. 10b)  
20 and a concomitant decrease in  $O_2$  and  $NO_3$  concentrations (Figs. 10a and 10c) around km 100  
21 reflect an increase in heterotrophic process rates that is mainly driven by the influence of the  
22 Rupel tributary.

23 Despite the overall agreement between model results and observations, Fig. 10 also reveals  
24 some discrepancies. For instance, the simulated  $O_2$ ,  $NH_4$  and  $dSi$  gradients are steeper than in

1 the observed profiles and simulated concentration minima are located further downstream.  
2 Part of this discrepancy can be explained by the highly dynamic nature of the estuarine  
3 environment and the strong inter-annual variability (e.g. Van Damme et al., 2005). Steady-  
4 state simulations forced with average summer conditions do not resolve such complex  
5 dynamics (e.g. Regnier et al., 1997; Arndt et al., 2009). Nevertheless, steady-state simulations  
6 results show that, despite numerous simplifying assumptions during model set-up, C-GEM is  
7 able to capture the general features of the biogeochemical dynamics in the Scheldt estuary.

#### 8 **4.4.3 Biogeochemical functioning**

9 Long-term seasonal to decadal biogeochemical dynamics or system-wide biogeochemical  
10 indicators, such as the NEM, are difficult to assess through observations only. Their  
11 quantification requires the application of fully-transient RTMs to complement field  
12 measurements (Regnier et al., 2013b). The quantification of such system-wide  
13 biogeochemical indicators provides an important integrative measure for the overall  
14 performance of C-GEM.

15 Therefore, the simulated annual evolution of spatially integrated NPP, aerobic degradation,  
16 denitrification, total heterotrophic degradation (denitrification and aerobic degradation),  
17 nitrification rates and NEM are compared to those obtained with the highly resolved 2D-RTM  
18 by Arndt et al. (2009). The integration is performed over the entire estuarine domain. Figure  
19 11 shows that C-GEM captures the main seasonal evolution of biogeochemical process rates.  
20 Autotrophic process rates are low during winter and autumn, but increase to a maximum in  
21 early summer (Fig. 11a), when favourable temperature and light conditions, large nutrient  
22 inventories and low turbidities drive high in-situ NPP rates. Heterotrophic process rates and  
23 nitrification are high during both winter and summer months (Figs. 11b-e). These high rates  
24 are sustained by high riverine inputs in winter and elevated ambient temperatures in summer

1 (Figs. 11b-e). In addition, **Figs. 11b-e show that** nitrification, denitrification and aerobic  
2 degradation are tightly coupled. For instance, high nitrification rates (**Fig. 11e**) are supported  
3 by the ammonium supplied by high aerobic degradation rates (**Fig. 11b**). **Moreover**, during  
4 summer, high nitrification and aerobic degradation rates result in a depletion of oxygen and,  
5 thus contribute to the increase in denitrification rates (Fig. 11c). Furthermore, heterotrophic  
6 degradation processes are enhanced by the supply of organic matter derived from dead  
7 phytoplankton in the aftermath of the summer algae bloom (Fig. 11d). Model results indicate  
8 that the heterotrophic degradation in the Scheldt is largely dominated by the aerobic organic  
9 matter degradation. The simulated NEM profile (Fig. 11f) closely follows the total  
10 heterotrophic degradation rate profile (Fig. 11d). During summer, the influence of  
11 heterotrophic processes on NEM is partly compensated by primary production rates (Fig.  
12 11a), but the simulated NEM remains negative throughout the year reflecting the  
13 heterotrophic nature of the estuary.

14 Although the idealized simulation performed with C-GEM captures the general seasonal  
15 pattern of system-wide process rates, Fig. 11 also reveals discrepancies between C-GEM and  
16 2D simulation results. **Whole-estuarine aerobic degradation rates are lower than those**  
17 **obtained with the 2-D model during** the first period of the year (day<60), while differences in  
18 NPP rates are more pronounced during the summer months. **Moreover, C-GEM simulates**  
19 **lower nitrification and denitrification rates.** These discrepancies can be traced back to  
20 differences in simulated water-depth, estuarine circulation, residence times and/or turbidity.  
21 The idealized geometry provides a highly simplified representation of the complex estuarine  
22 bathymetry with deep tidal channels and extensive intertidal mud flats. As a consequence, C-  
23 GEM ignores the cross-sectional variability in water depth, circulation and, thus, residence  
24 times. For instance, C-GEM underestimates residence times in the upper reaches and,  
25 therefore, simulates lower **biogeochemical rates.** **These cross-sectional variabilities in**

1 residence time, turbidity and residual circulation exert also an important influence on summer  
2 NPP rates. Two-dimensional simulation results highlight the pronounced differences between  
3 NPP rates in tidal channels and intertidal flats (e.g. Arndt and Regnier, 2007), a feature that  
4 cannot be resolved by the idealized bathymetry of C-GEM. The simplification of the estuarine  
5 bathymetry may thus explain also the observed differences in simulated NPP rates. In  
6 addition, C-GEM simulates lower nitrification rates but slightly higher aerobic degradation  
7 rates during the summer months. These discrepancies probably arise from different estimates  
8 of the transient overlap in  $TOC$  and  $O_2$  for aerobic degradation and in  $NH_4$  and  $O_2$  for  
9 nitrification, which induce different values of the Michaelis-Menten terms involved in these  
10 two processes-

11 Despite these discrepancies, integrated biogeochemical reaction rates estimated with C-GEM  
12 concur well with the 2D results. Annually integrated biogeochemical process rates are  
13 compared in Fig. 12. C-GEM slightly underestimates nitrification, denitrification and aerobic  
14 degradation rates, as well as the oxygen exchange with atmosphere with a relative error of  
15 36%, 24%, 4% and 17%, respectively. Simulated NPP rates are slightly higher with a relative  
16 error of 23%, while the simulated NEM value is slightly lower by about 10%. Thus, all  
17 integrated measures fall within the same order of magnitude.

#### 18 **4.5 Sensitivity analysis**

19 Figure 13 illustrates the sensitivity of biogeochemical process rates to parameter variations  
20 (Table 7). Geometrical parameters generally exert an important influence on all integrated  
21 process rates (Fig. 13a). For instance, a 10% variation in convergence length ( $LC$ ) triggers  
22 large changes (>15%) in NPP, aerobic degradation and nitrification rates and also exerts a  
23 somewhat smaller influence (~10%) on denitrification and air/water exchange rates. This  
24 difference is system specific and can be explained by the effect of convergence length on

1 estuarine volume and residence time (Eqs. (1) and (2)). Fixing the estuarine width,  $B$ , at the  
2 inland limit, as done during this sensitivity test and following Eq. (2), a shorter convergence  
3 length increases the volume and the residence time in the estuarine system, a central  
4 parameter that in turn promote all process and increases their biogeochemical rates (Fig. 13a).  
5 A larger convergence length has the opposite effect on the rates. Denitrification is the most  
6 sensitive process to variations in water depth,  $H$  (Fig. 13a). The volumetric reduction of the  
7 estuary induced by a shallower water depth translates into a decrease in aerobic degradation,  
8 denitrification and nitrification rates. The large reduction in denitrification may also be related  
9 to the positive effect of shallow water depth on oxygen exchange rate, which inducing an  
10 increase in  $O_2$  levels in the water column strongly inhibits denitrification. The increase in  
11 NPP rates to both positive and negative relative variations in water depth highlights the strong  
12 dependence of this process on the underwater light field. Shallow waters increase the photic  
13 depth to water depth ratio, while deep waters decrease light attenuation through a dilution  
14 effect on suspended sediment concentrations (results not shown; Chen et al., 2005; Desmit et  
15 al., 2005). Despite their strong influence on biogeochemical processes, estuarine geometric  
16 features do not limit the application of C-GEM to data-poor estuarine systems, since they can  
17 be readily extracted from nautical charts or maps.

18 Integrated NPP rates are also highly sensitive to variations in primary production and SPM  
19 parameters (Figs. 13b and 13e), while they are not affected by variations in gas exchange  
20 parameter and biogeochemical rate constants (Figs. 13c and 13d). This reflects the fact that  
21 underwater light field rather than nutrient availability controls NPP. As a consequence, NPP  
22 is also sensitive to changes in the Chézy coefficient,  $C$  (>66%), which affect SPM dynamics  
23 and, thus, the light availability, and in phytoplankton parameters (Fig. 13e). Variations in the  
24 maintenance rate constant exert the largest influence on system-wide integrated NPP (>77%)  
25 because the maintenance term is directly proportional to the total phytoplankton concentration

1 (see Table 1). Although both growth and excretion are linearly proportional to gross primary  
2 production, the integrated NPP only respond to variations in the growth constant because its  
3 value is one order of magnitude larger than that of the excretion constant. Photosynthesis  
4 efficiency also has a significant effect on NPP variations as shown in Fig. 13b and integrated  
5 rates vary by as much as 53%. Overall, simulation results indicate that NPP rates are most  
6 sensitive to uncertainties in the Chézy coefficient and the rate constant for maintenance.  
7 These parameter values are difficult to determine and are generally obtained from model  
8 calibration. In particular, the Chézy coefficient is never measured directly, while the  
9 maintenance term generally varies across different phytoplankton groups. Heterotrophic and  
10 oxygen exchange rates are most sensitive to variations in biogeochemical reaction rate  
11 constants (Fig. 13d) and to a lesser degree variations in the current component for the piston  
12 velocity (Fig. 13c) and in the Chézy coefficient (Fig. 13e). On the other hand, NPP  
13 parameters exert virtually no effect (Fig. 13b), emphasizing the strongly heterotrophic  
14 character of the estuarine system (Figs. 11 and 12). While aerobic degradation and  
15 nitrification show only small variations (<10%) associated to changes in the current  
16 contribution to the piston velocity, Fig. 13c confirms the sensitivity of denitrification to the  $O_2$   
17 exchange process at the air-water interface and to the  $O_2$  level in water. To a variation in gas  
18 exchange rate corresponds an opposite variation in denitrification. Hence, estimates of these  
19 two processes require a good resolution of the flow velocity field and the water depth in order  
20 to well constrain the flow component for the piston velocity.

21 Simulation results emphasize that a robust quantitative estimation of the estuarine  
22 biogeochemical functioning calls for well-constrained biogeochemical rate constants.  
23 However, these constants are difficult to constrain as they implicitly account for factors that  
24 are not resolved in C-GEM, such as the structure and the abundance of the microbial  
25 community or a complete description of the environmental conditions within the estuarine

1 systems. The lack of an objective framework for model parameterization and the limited  
2 transferability of system-specific parameter values potentially may limit the generic approach  
3 of C-GEM. Hence, a sensitivity study should be an integral part of the model application and  
4 can help to estimate uncertainties in predicted rates.

5 Despite the relatively large variations applied in the sensitive runs, the estuary never becomes  
6 net autotrophic and NEM always remains negative within the range -6235 and -10461 kmol C  
7  $\text{d}^{-1}$ . Figure 14 identifies the parameters that lead to a NEM variation larger than 5%. Since the  
8 NEM is always negative, a positive relative variation in its value implies a more heterotrophic  
9 status of the system. These results again highlight that an increase in volume and, thus, in  
10 residence time (induced by a decrease in  $LC$  and by an increase in depth; see above) and in  
11 aerobic degradation rate constant induce a more negative NEM, while an increase in  $LC$  and a  
12 decrease in depth and aerobic degradation constant rate have the inverse effect. A comparison  
13 of Fig. 14 with Figs. 13a and 13d shows that variations in NEM closely follow the variations  
14 in aerobic degradation, induced by these 3 parameters ( $LC$ ,  $H$ ,  $k_{ox}$ ), reflecting the overall  
15 dominance of this process in the NEM estimates.

16 Note that, while the general pattern emerging from this sensitivity study is valid across  
17 systems, the quantitative influence of parameter variations is highly system-dependent. For  
18 instance, prismatic system with a longer convergence length and, thus, a stronger fluvial  
19 influence are characterized by much shorter residence times. Therefore, integrated  
20 biogeochemical reaction rates in prismatic systems will, likely, reveal a much weaker  
21 response to variations in biogeochemical parameters than in funnel-shaped systems.

22

## 23 **5 Scope of Applicability and Model Limitations**

24 Site-specific, multi-dimensional models generally perform satisfactorily at reproducing the

1 biogeochemical dynamics of estuarine systems, but are highly-demanding in terms of data  
2 and numerical requirements. At the other end of the model spectrum, box models are very  
3 efficient, but generally fail to resolve the spatial and temporal variability of estuarine systems  
4 and are not well suited for model-data comparison. However, our ability to assess the role of  
5 the estuarine environment for global biogeochemical cycles and greenhouse gas budgets, as  
6 well as their response to ongoing global change requires tools that are computationally  
7 efficient and can extrapolate knowledge from well-studied to data-poor systems, while at the  
8 same time resolving the most important hydrodynamic and biogeochemical processes and  
9 scales. The new one-dimensional model C-GEM proposed here is such a computational tool.  
10 It represents a valid compromise between performance and computational efficiency and  
11 reduces data-requirements by using an idealized representation of the estuarine geometry. Its  
12 scope of applicability covers the entire range of alluvial estuaries, from tidally-dominated  
13 systems with a large tidal range and low river discharge to fluvial-dominated systems  
14 characterized by significant freshwater input (Regnier et al., 2013b). It can be used to resolve  
15 the complex process interplay that drives the estuarine biogeochemical dynamic and to  
16 quantify estuarine carbon and nutrient budgets. In addition, the computational efficiency of C-  
17 GEM offers the possibility to simulate simultaneously the biogeochemical dynamics of a  
18 large number of estuaries and the contiguous coastal ocean. Although not considered so far,  
19 C-GEM could theoretically be applied to the tidally-influenced, inland sections of very large  
20 river systems (e.g. Amazon). The value of such application is however questionable because  
21 very large rivers contribute disproportionately to the overall land to ocean carbon fluxes and  
22 might thus deserve a dedicated model. In addition, their tight estuarine-continental shelf  
23 coupling and the importance, as well as, the complex multi-dimensional dynamics of their  
24 coastal plumes requires a multi-dimensional model representation. Numerous models have  
25 already been developed for these systems (e.g. Gallo and Vinzon, 2005; Denamiel et al.,

1 2013) and in the future, they could be explicitly represented in high-resolution Earth System  
2 Models (Bauer et al., 2013). In contrast, for the smaller alluvial estuarine systems,  
3 mechanistically rooted upscaling strategies need to be designed to better constrain their roles  
4 in the global carbon cycle (Bauer et al., 2013) and C-GEM is a tool of choice in this context.  
5 However, C-GEM is associated with a certain degree of simplification and, therefore, is  
6 characterized by some limitations. Currently, the model does not include a benthic-pelagic  
7 exchange module. Hence, its application is not recommended for estuaries that are subject to  
8 an intense benthic-pelagic coupling. The resulting lack of a representation of particulate  
9 organic carbon burial might result in an overestimation of estuarine organic carbon export  
10 fluxes to the coastal ocean. The most important hurdle towards generalisation arises from the  
11 lack of an objective, global framework for SPM and biogeochemical process  
12 parameterization. These parameters implicitly account for a large number of controlling  
13 factors that are usually not explicitly resolved in estuarine models. They are typically derived  
14 by model calibration on the basis of observations and their transferability to other systems is  
15 thus limited. Comprehensive sets of model parameters are now available for some estuaries of  
16 the world, such as those in Europe, North America and Australia, but are essentially missing  
17 in the tropical and polar regions (Regnier et al., 2013b). The limited transferability of model  
18 parameters and the lack of observational data calls for the creation of a global dataset of  
19 estuarine sediment and biogeochemical parameters, on which a statistical analysis is strongly  
20 desirable in order to identify common trends and possible relationships between parameters  
21 and control factors, such as latitude, catchment characteristics and anthropic pressure.

22

## 23 **6 Conclusion and perspectives**

1 The model developed in this study represents a first attempt to quantify the biogeochemical  
2 dynamics in estuaries using a one-dimensional reactive-transport model that relies on  
3 idealized geometries to support the estuarine hydrodynamics and transport. Despite its highly  
4 simplified geometric support, C-GEM captures the dominant features of the biogeochemical  
5 behavior along a complex system as the Scheldt estuary (BE/NL) and the system-wide  
6 integrated reaction rates for the main biogeochemical pelagic processes are comparable with  
7 those obtained using a high-resolved site-specific 2D-RTM. A sensitivity analysis, based on  
8 the OFAT method, has been performed in order to assess the importance of the internal  
9 parameters on the estuarine biogeochemistry. It reveals that geometry and hydrodynamics  
10 exert a strong first-order control on the biogeochemical functioning and supports therefore our  
11 hypothesis that the estuarine response is a system-specific attribute that cannot be reduced to a  
12 simple and direct signal-response, such as the nutrient filtering capacity and the residence  
13 time relationship proposed, for instance, by Nixon et al. (1996). Results also provide a  
14 rational support to identify the model parameters that are the most sensitive with respect to  
15 integrative measures, such as the NEM, and emphasize the need for a global compilation of  
16 estuarine sediment and biogeochemical parameters. In addition, such compilation could help  
17 identify trends between parameter values and control factors, such as climate, catchment  
18 properties and anthropic pressure, and compensate for the current lack of an objective, global  
19 framework for parameterization in data-poor areas.

20 The structure of C-GEM, which optimizes the ratio between the number of parameters and the  
21 availability of data, provides an easy and cost-efficient tool that can be used to quantify the  
22 biogeochemical dynamics of estuaries and to forecast their response to combined climate and  
23 environmental changes over the coming century. In the future, C-GEM could be applied, in  
24 combination with, for example, GlobalNEWS2 models (Mayorga et al., 2010) for riverine  
25 inputs, to a wide range of estuarine systems characterized by different climatic regimes,

1 geometries and chemical loadings. This, together with the compilation of a global dataset for  
2 sediment and biogeochemical parameters, could help in the quantification of estuarine  
3 biogeochemical cycles at regional and global scales.

4

## 5 **7 Code Availability**

6 The C-GEM source code related to this article is provided as supplementary package together  
7 with a Read Me file, where hardware and software requirements, source code files and model  
8 output files management are fully described.

9

## 1 **References**

- 2 **Abril G., Nogueira M., Etcheber H., Cabeçadas G., Lemaire E., and Brogueira M. J.:**  
3 **Behaviour of Organic Carbon in Nine Contrasting European Estuaries. *Estuar. Coastal Shelf***  
4 ***S.*, 54, 241-262, 2002**
- 5 Alongi D. M.: Coastal Ecosystem Processes, 1st edition, CRC Marine Science Series,  
6 Kennish M. J. and Lutz P. L. (Eds.), CRC PressI, New York, USA, 1998
- 7 Alpine A. E. and Cloern J. E.: Trophic interactions and direct physical effects control  
8 phytoplankton biomass and production in an estuary, *Limnol. Oceanogr.*, 37, 946-955, 1992
- 9 Andersson A. J. and Mackenzie F. T.: Shallow-water ocean: A source or sink of atmospheric  
10 CO<sub>2</sub>?, *Front. Ecol. Environ.*, 2, 348-353, 2004
- 11 **Andersson A. J., MacKenzie F. T., and Lerman A.: Coastal ocean and carbonate systems in**  
12 **the high CO<sub>2</sub> world of the anthropocene, *Am. J. Sci.*, 305, 875–918, 2005.**
- 13 Andersson M. G. I., Brion N. and Middelburg, J. J.: Comparison of nitrifer activity versus  
14 growth in the Scheldt estuary: a turbid tidal estuary in northern Europe, *Aquat. Microb. Ecol.*,  
15 42, 149-158, 2006
- 16 Arndt S., Vanderborcht J. P. and Regnier P.: Diatom growth response to physical forcing in a  
17 macrotidal estuary: Coupling hydrodynamics, sediment transport and biogeochemistry, *J.*  
18 *Geophys. Res.*, 112, C05045, doi:10.1029/2006JC003581, 2007
- 19 Arndt S. and Regnier P.: A model for the benthic-pelagic coupling of silica in estuarine  
20 ecosystem: Sensitivity analysis and system scale simulation, *Biogeosciences*, 4, 1-22, 2007
- 21 Arndt S., Regnier P. and Vanderborcht J. P.: Seasonally-resolved nutrient filtering capacities  
22 and export fluxes in a macrotidal estuary, *J. Marine Syst.*, 78, 42-58, 2009

- 1 Arndt S., Lacroix G., Gypens N., Regnier P. and Lancelot C: Nutrient dynamics and  
2 phytoplankton development along an estuary-coastal zone continuum: A model study, J.  
3 Marine Syst., 84, 49-66, 2011
- 4 Arndt, S., Jorgensen, B., LaRowe, D., Middelburg, J., Pancost, R., and Regnier, P.:  
5 Quantification of organic matter degradation in marine sediments: A synthesis and  
6 review, *Earth-Sci. Rev.*, 123, 53-86, 2013
- 7 Atlas R., Hoffman R. N., Ardizzone J., Leidner S. M., Jusem J. C., Smith D. K. and Gombos  
8 D.: A cross-calibrated multiplatform ocean surface wind velocity product for meteorological  
9 and oceanographic applications, *Bull. Amer. Meteor. Soc.*, 92, 157-174, 2011
- 10 Baklouti M., Chevalier C., Bouvy M., Corbin D., Pagano M., Troussellier M. and Arfi R.: A  
11 study of plankton dynamics under osmotic stress in the Senegal River Estuary, West Africa,  
12 using a 3D mechanistic model, *Ecol. Model.*, 222, 2704-2721, 2011
- 13 Bauer J. E., Cai W.-J., Raymond P. A., Bianchi T. S., Hopkinson C. S. and Regnier P. A. G.:  
14 The Coastal Ocean as a Key Dynamic Interface in the Global Carbon Cycle, *Nature*, 504, 61-  
15 70, 2013
- 16 Benson B. B. and Krause D. Jr.: The concentration and isotopic fractionation of oxygen  
17 dissolved in freshwater and seawater in equilibrium with the atmosphere, *Limnol. Oceanog.*,  
18 29, 620-632, 1984
- 19 Billen G., Somville M., De Becker E. and Servais P.: A nitrogen budget of the Scheldt  
20 hydrographical basin, *Neth. J. Sea Res.*, 19, 223-230, 1985
- 21 Billen G., Garnier J. and Hanset P.: Modelling phytoplankton development in whole drainage  
22 networks: the RIVERSTRAHLER Model applied to the Seine river system, *Hydrobiologia*,  
23 289, 199-137, 1994

- 1 Billen G. and Garnier J.: The Phison River plume: coastal eutrophication in response to  
2 change in land use and water management in the watershed, *Aquat. Microb. Ecol.*, 13, 3-17,  
3 1997
- 4 Billen G., Garnier J. and Rousseau V.: Nutrient fluxes and water quality in the drainage  
5 network of the Scheldt basin over the last 50 years. *Hydrobiol*, 540, 47-67, 2005
- 6 Borges A. V. and Abril G.: Carbon Dioxide and Methane Dynamics in Estuaries, *Treatise on*  
7 *Estuarine and Coastal Science*, 5, 119-161, 2011
- 8 Bowers D. G., Boudjelas S. and Harker G. E. L.: The distribution of fine suspended sediments  
9 in the surface waters of the Irish Sea and its relation to tidal stirring, *Int. J. Remote Sens.*, 19,  
10 2789-2805, 1998
- 11 Brion N., Andersson M. G. I., Elskens M., Diaconu C., Bayens W., Dehairs F. and  
12 Middelburg J. J.: Nitrogen cycling, retention and export in a eutrophic temperate macrotidal  
13 estuary, *Mar. Ecol-Prog Ser.*, 357, 87-99, 2008
- 14 Brock T. D.: Calculating solar radiation for ecological studies, *Ecol. Model.*, 14, 1-19, 1981
- 15 Cancino L. and Neves R.: Hydrodynamic and sediment suspension modelling in estuarine  
16 systems Part I: Description of the numerical models, *J. Marine Syst.*, 22, 105-116, 1999
- 17 Cazenave A. and Savenije H.: Preface to the Special Issue on "Hydrology from Space,  
18 *Surveys in Geophysics*, 29, 241-245, 2008
- 19 Cerco C. F. and Cole T. M.: Three-Dimensional Eutrophication Model of Chesapeake Bay,  
20 Technical Report EL-94-4, U.S. Environmental Protection Agency and U.S. Army Engineer  
21 District, Baltimore, 1994

- 1 Cerco C. F., Tillman D. and Hagy J. D.: Coupling and comparing a spatially- and temporally-  
2 detailed eutrophication model with an ecosystem network model: An initial application to  
3 Chesapeake Bay, *Environ. Modell. Softw.*, 25, 562-575, 2010
- 4 Chen M. S.: Suspended matter and flocculation in the estuarine environment, Ph.D. Thesis,  
5 Vrije Universiteit Brussels, Belgium, 2003
- 6 Chen M. S., Wartel S., Eck B. and Van Maldegem D. C.: Suspended matter in the Scheldt  
7 estuary, *Hydrobiologia*, 540, 79-104, 2005
- 8 Crossland C. J., Kremer H. H. and Lindeboom H. J., Marshall Crossland J. I. and Le Tissier  
9 M. D. A. (Eds.): Coastal Fluxes in the Anthropocene, 1st edition, Global Change - The IGBP  
10 Series, Springer, Berlin, 2005
- 11 Dalrymple R. W., Zaitlin B. A. and Boyd R.: Estuarine facies models: Conceptual basis and  
12 stratigraphic implications, *J. Sediment. Petrol.*, 62, 1130-1146, 1992
- 13 Davies J. L.: A morphogenic approach to world shore-lines, *Zeitschrift fur Geomorphologie*,  
14 8, 127-142, 1964
- 15 Denamiel C., Budgell W. P., and Toumi R.: The Congo River plume: Impact of the forcing on  
16 the far-field and near-field dynamics, *J. Geophys Res-Oceans*, 118, 964-989, 2013.
- 17 Desmit X., Vanderborcht J. P., Regnier P. and Wollast R.: Control of phytoplankton  
18 production by physical forcing in a strongly tidal, well-mixed estuary, *Biogeosciences*, 2,  
19 205-218, 2005
- 20 Doxaran D., Froidefond J. M., Lavender S. and Castaing P.: Spectral signature of highly  
21 turbid waters: Application with SPOT data to quantify suspended particulate matter  
22 concentrations, *Remote Sens. Environ.*, 81, 149-161, 2002

- 1 Doxaran D., Froidefond J. M., Castaing P. and Babin M.: Dynamics of the turbidity  
2 maximum zone in a macrotidal estuary (the Gironde, France): Observations from field and  
3 MODIS satellite data, *Estuari. Coast. Shelf S.*, 81, 321-332, 2009
- 4 Dürr H. H., Laruelle G. G., Van Kempen C. M., Slomp C. P., Maybeck M. and Middelkoop  
5 H.: World-wide typology of near-shore coastal systems: defining the estuarine filter of river  
6 inputs to the oceans, *Estuaries Coasts*, 34, 441-458, 2011
- 7 Dyer K. R. (Ed.): *Estuaries: A physical introduction*, 2nd edition, Wiley, Chichester, 1973
- 8 Dyer K. R. (Ed.): *Coastal and Estuarine Sediment Dynamics*, Wiley & Sons, Chichester, 1986
- 9 Einstein H. B. and Krone R. B.: Experiments to determine modes of cohesive sediment  
10 transport in salt water, *J. Geophys. Res.*, 67, 1451-1461, 1962
- 11 Fekete B. M., Vörösmarty C. J. and Grabs W.: High-resolution fields of global runoff  
12 combining observed river discharge and simulated water balances, *Global Biogeochem. Cy.*,  
13 16, 815-827, 2002
- 14 Fischer H. B.: Mixing and Dispersion in Estuaries, *Annu. Rev. Fluid Mech.*, 8, 107-133, 1976
- 15 Fettweis M. P. and Nechad B.: Evaluation of in situ and remote sensing sampling methods for  
16 SPM concentrations, Belgian continental shelf (southern North Sea), *Ocean Dynam.*, 61, 157-  
17 171, 2011
- 18 Friedrichs A. M. and Hofmann E. E.: Physical controls of biological processes in the central  
19 Equatorial Pacific Ocean, *Deep-Sea Res. I*, 48, 1023-1069, 2001
- 20 Gallo M. N. and Vinzon S. B.: Generation of overtides and compound tides in Amazon  
21 estuary, *Ocean Dynam.*, 55, 441-448, 2005.
- 22 Gao J.: Bathymetric mapping by means of remote sensing: methods, accuracy and limitations,  
23 *Prog. Phys. Geog.*, 33, 103-116, 2009

- 1 Garnier J., Billen G. and Coste M.: Seasonal succession of diatoms and Chlorophyceae in the  
2 drainage network of the Seine River: Observations and modelling, *Limnol. Oceanogr.*, 40,  
3 750-765, 1995
- 4 Garnier J., Némery J., Billen G. and Théry S.: Nutrient dynamics and control of  
5 eutrophication in the Marne River system: modelling the role of exchangeable phosphorus, *J.*  
6 *Hydrol.*, 304, 397-412, 2005
- 7 Gattuso J. P., Frankignoulle M. and Wollast R.: Carbon and Carbonate Metabolism in Coastal  
8 Aquatic System, *Annu. Rev. Ecol. Syst.*, 29, 405-434, 1998
- 9 Geyer W. R., Morris J. T., Prahl G., Jay D. A. and Turner E.: Interaction between physical  
10 processes and ecosystem structure: a comparative approach, in: *Estuarine Science: A*  
11 *synthetic approach to research and practice*, Hobbie J. E. (Ed.), Island Press, Washington,  
12 177-206, 2000
- 13 Gypens N., Lancelot C. and Soetaert K.: Simple parameterisations for describing N and P  
14 diagenetic processes: Application in the North Sea, *Prog. Oceanogr.*, 76, 89-110, 2008
- 15 Gypens N., Delhez E., Vanhoutte-Brunier A., Burton S., Thieu V., Passy P., Liu Y., Callens  
16 J., Rousseau V. and Lancelot C.: Modelling phytoplankton succession and nutrient transfer  
17 along the Scheldt estuary (Belgium, The Netherlands), *J. Marine Syst.*, **128, 89-105, 2013**
- 18 Hansen D. V. and Rattray M.: New dimensions in estuary classification, *Limnol. Oceanogr.*,  
19 11, 319-326, 1966
- 20 Hellings L. and Dehairs F.: Dissolved inorganic carbon in a highly polluted estuary (the  
21 Scheldt), *Limnol. Oceanogr.*, 46, 1406-1414, 2001

1 Hofmann A. F., Soetaert K. and Middelburg J. J.: Nitrogen and carbon dynamics in the  
2 Scheldt estuary at the beginning of the 21st century - a modelling study, *Biogeosciences*  
3 *Discussions*, 5, 83-161, 2008

4 Horrevoets A. C., Savenije H. H. G., Schuurman J. N. and Graas S.: The influence of river  
5 discharge on tidal damping in alluvial estuaries, *J. Hydrol.*, 294, 213-228, 2004

6 Ippen A. T. and Harleman D. R. F.: *One-dimensional Analysis of Salinity Intrusion in*  
7 *Estuaries*, Technical Bulletin No. 5, Committee on Tidal Hydraulics, Corps of Engineers, U.  
8 S. Army, Vicksburg, 1961

9 IRM: *Observations climatologiques - Bulletin mensuel de l'Institut Royale Météorologique de*  
10 *Belgique*, Marcorps, H. (Ed.), 2004

11 Jahnke R. A., Emerson S. R. and Murray J. W.: A model of oxygen reduction, denitrification  
12 and organic matter mineralization in marine sediments, *Limnol. Oceanogr.*, 27, 610-623, 1982

13 Jahnke R. A.: The global ocean flux of particulate organic carbon: areal distribution and  
14 magnitude, *Global Biogeochem. Cy.*, 10, 71-88, 1996

15 Jay D. A., Giese B. S. and Sherwood C. R.: Energetics and sedimentary processes in the  
16 Columbia River estuary, *Progr. Oceanogr.*, 25, 157-174, 1990

17 Jay D. A., Geyer W. R. and Montgomery D. R.: An ecological perspective on estuarine  
18 classification, in: *Estuarine science: A synthetic approach to research and practice*, Hobbie J.  
19 E. (Ed.), Island Press, Washington, 149-176, 2000

20 Jiao N., Tank K., Cai H. and Mao Y.: Increasing the microbial carbon sink in the sea by  
21 reducing chemical fertilization on the land, *Nat. Rev. Microbiol.*, 9, 75-75, 2011

22 Kent B. H.: *Turbulent diffusion in a Sectionally Homogeneous Estuary*, Technical Report 16,  
23 Chesapeake Bay Institute, John Hopkins University, Baltimore, 1958

1 Lancelot C., Hannon E., Becquevort S., Veth C. and de Baar H. J. W.: Modeling  
2 phytoplankton blooms and carbon export production in the Southern Ocean: Dominant  
3 controls by light and iron in the Atlantic sector in Austral spring 1992, *Deep-Sea Res. I*, 47,  
4 1621-1662, 2000

5 Langdon C.: The significance of respiration in production measurements based on oxygen, in:  
6 *ICES Marine Science Symposium 197:69-78*, 1993

7 Laruelle G. G., Roubex V., Sferratore A., Brodherr B., Ciuffa D., Conley D. J., Dürr H. H.,  
8 Garnier J., Lancelot C., Le Thi Phuong Q., Meunier J. D., Meybeck M., Michalopoulos P.,  
9 Moriceau B., Ní Longphuirt S., Loucaides S., Papush L., Presti M., Ragueneau O., Regnier P.  
10 A. G., Saccone L., Slomp C. P., Spiteri C. and Van Cappellen P.: The global biogeochemical  
11 cycle of silicon: role of the land-ocean transition and response to anthropogenic perturbation,  
12 *Global Biogeochem. Cy.*, 23, GB4031, doi: 10.1029/2008GB003267, 2009

13 Laruelle G. G.: Quantifying nutrient cycling and retention in coastal waters at the global  
14 scale, Ph.D. Thesis, Universiteit Utrecht, The Netherlands, 2009

15 Le Pape O., Jean F. and Menesguen A.: Pelagic and benthic trophic chain coupling in a semi-  
16 enclosed coastal system, the Bay of Brest (France): a modelling approach, *Mar. Ecol.-Prog.*  
17 *Ser.* 189, 135-147, 1999

18 Leonard B.: Third-Order Upwinding as a Rational Basis for Computational Fluid Dynamics,  
19 in: *Computational Techniques and Applications: CTAC-83*, Noye J. and Fletcher C. A. J.  
20 (Eds.), Elsevier, North-Holland, 1984

21 Lin J., Xie L., Pietrafesa L. J., Ramus J. S. and Paerl H. W.: Water Quality Gradients across  
22 Albemarle-Pamlico Estuarine System: Seasonal Variations and Model Applications, *J.*  
23 *Coastal Res.*, 23, 213-229, 2007

- 1 Liu K. K., Atkinson L., Quinones R. and Talaue-McManus L. (Eds.): Biogeochemistry of  
2 continental margins in a global context, in: Carbon and Nutrient Fluxes in Continental  
3 Margins: A Global Synthesis, IGBP Book Series, Springer, Berlin, Germany, 3-24, 2010
- 4 Mackenzie F. T., Lerman A., and DeCarlo E. H.: Coupled C, N, P, and O biogeochemical  
5 cycling at the land-ocean interface. In: Treatise on Coastal and Estuarine Science, v. 5, J.  
6 Middleburg and R. Laane, eds., Elsevier, 317-342, 2012.
- 7 Maris T., Van Damme S. and Meire P.: Onderzoek naar de gevolgen van het Sigmaplan,  
8 baggeractiviteiten en havenuitbreiding in de Zeeschelde op het milieu, Geïntegreerd  
9 eindverslag van het onderzoek verricht in 2003, Universiteit Antwerpen, Belgium, 2004
- 10 Mayorga E. and Seitzinger S. P. and Harrison J. A. and Beusen A. H. W. and Bouwman A. F.  
11 and Fekete B. M. and Kroze C. and Van Drecht G.: Global Nutrient Export from Watersheds  
12 2 (NEWS 2): Model development and implementation, Environ. Modell. Softw., 25, 837-853,  
13 2010
- 14 Mehta A., Hayter E., Parker W., Krone R. and Teeter A.: Cohesive Sediment Transport. I:  
15 Process Description, J. Hydraul. Eng.-ASCE, 115, 1076-1093, 1989
- 16 Meire P., Ysebaert T., Van Damme S., Van der Bergh E., Maris T. and Struyf E.: The Scheldt  
17 estuary: A description of a changing ecosystem, Hydrobiologia, 540, 1-11, 2005
- 18 Monbet Y.: Control of phytoplankton biomass in estuaries: A comparative analysis of  
19 microtidal and macrotidal estuaries, Estuaries, 15, 563-571, 1992
- 20 Moore G. F., Aiken J. and Lavender S. J.: The atmospheric correction of water colour and the  
21 quantitative retrieval of suspended particulate matter in Case II waters: application to MERIS,  
22 Int. J. Remote Sens., 20, 1713-1733, 1999

- 1 Muylaert K. and Sabbe K.: Spring phytoplankton assemblages in and around the maximum  
2 turbidity zone of the estuary of the Elbe (Germany), the Schelde (Belgium/Netherlands) and  
3 the Gironde (France), *J. Marine Syst.*, 22, 133-149, 1999
- 4 Nguyen A. D.: Salt intrusion, tides and mixing in multi-channel estuaries, Ph.D. Thesis,  
5 Taylor and Francis/Balkema, The Netherlands, 2008
- 6 Nielsen K., Nielsen L. P. and Rasmussen P.: Estuarine nitrogen retention independently  
7 estimated by the denitrification rate and mass balance methods: A study of Nnorsminde Fjord,  
8 Denmark, *Mar. Ecol.-Prog. Ser.*, 119, 275-283, 1995
- 9 Nihoul J. C. J. and Ronday F.: Modèles d'estuaires partiellement stratifiés, *Projet Mer*, Vol.  
10 10, Service de la Programmation Scientifique, Bruxelles, Belgium, 71-98, 1976
- 11 Nixon S. W., Ammerman J. W., Atkinson L. P., Berounsky V. M., Billen G., Boicourt W. C.,  
12 Boynton W. R., Church T. M., Ditoro D. M., Elmgren R., Garber J. H., Giblin A. E., Jahnke  
13 R. A., Owens N. J. P., Pilson M. E. Q. and Seitzinger S. P.: The fate of nitrogen and  
14 phosphorus at the land-sea margin of the North Atlantic Ocean, *Biogeochemistry*, 35, 141-  
15 180, 1996
- 16 Odum H. T.: Primary Production in Flowing Waters, *Limnol. Oceanogr.*, 1, 102-117, 1956
- 17 O'Kane J. P.: *Estuarine Water-quality Management*, Pitman Publishing, London, 1980
- 18 Paerl H. W., Valdes L. M., Peierls B. L., Adolf J. E. and Harding L. W. Jr.: Anthropogenic  
19 and climatic influences on the eutrophication of large estuarine ecosystems, *Limnol.*  
20 *Oceanogr.*, 51, 448-462, 2006
- 21 Park K., Jung H.-S., Kim H.-S., Ahn S.-M.: Three-dimensional hydrodynamic-eutrophication  
22 model (HEM-3D): application to Kwang-Yang Bay, Korea, *Mar. Environ. Res.*, 60, 171-193,  
23 2005

- 1 Partheniades E.: A study of erosion and deposition of cohesive soils in salt water, Ph. D.
- 2 Thesis, University of California, USA, 1962
- 3 Pethick J.: An introduction to coastal geomorphology, Arnold E. (Ed.), London, 1984
- 4 Prandle D.: The influence of bed friction and vertical eddy viscosity on tidal propagation,
- 5 Cont. Shelf Res., 17, 1367-1374, 1985
- 6 Preddy W. S.: The mixing and movement of water in the estuary of the Thames, J. Mar. biol.
- 7 Ass. U.K., 33, 645-662, 1954
- 8 Press W. H., Teukolosky S. A., Vetterling W. T. and Flannery B. P.: Numerical Recipes in C:
- 9 The Art of Scientific Programming, 2nd edition, Cambridge University Press, USA, 1992
- 10 Pritchard D. W.: Estuarine circulation patterns, Proceedings of the American Society of Civil
- 11 Engineering, 81, 1-11, 1955
- 12 Pritchard D. W.: The Equations of Mass Continuity and Salt Continuity in Estuaries, J.
- 13 Marine Res., 15, 33-42, 1958
- 14 Rabouille C., Mackenzie F. T. and Ver L. M.: Influence of the human perturbation on carbon,
- 15 nitrogen, and oxygen biogeochemical cycles in the global coastal ocean, Geochim.
- 16 Cosmochim. Ac., 65, 3615-3641, 2001
- 17 Regnier P., Wollast R. and Steefel C. I.: Long-term fluxes of reactive species in macrotidal
- 18 estuaries: Estimates from a fully transient, multicomponent reaction-transport model, Mar.
- 19 Chem., 58, 127-145, 1997
- 20 Regnier P., Mouchet A., Wollast R. and Ronday F.: A discussion of methods for estimating
- 21 residual fluxes in strong tidal estuaries, Cont. Shelf Res., 18, 1543-1571, 1998

1 Regnier P. and Steefel C. I.: A high resolution estimate of the inorganic nitrogen flux from the  
2 Scheldt estuary to the coastal North Sea during a nitrogen-limited algal bloom, spring 1995,  
3 *Geochim. Cosmochim. Ac.*, 63, 1359-1374, 1999

4 Regnier P., Vanderborght J. P., Steefel C. I. and O'Kane J. P.: Modeling complex multi-  
5 component reactive-transport systems: Towards a simulation environment based on the  
6 concept of a Knowledge Base, *Appl. Math. Model.*, 26, 913-927, 2002

7 Regnier P., Slomp C. and Jourabchi P.: Reactive transport modeling as a technique for  
8 understanding coupled biogeochemical processes in surface and subsurface environments,  
9 *Neth. J. Geosci.*, 82, 5-18, 2003

10 Regnier P., Friedlingstein P., Ciais P., Mackenzie F. T., Gruber N., Janssens I. A., Laruelle G.  
11 G., Lauerwald R., Luysaert S., Andersson A. J., Arndt S., Arnosti C., Borges A. V., Dale A.  
12 W., Gallego-Sala A., Godd ris Y., Goossens N., Hartmann J., Heinze C., Ilyina T., Joos F.,  
13 LaRowe D. E., Leifeld J., Meysman F. J. R., Munhoven G., Raymond P. A. , Spahni R.,  
14 Suntharalingam P. and Thullner M.: Anthropogenic perturbation of the carbon fluxes from  
15 land to ocean, *Nat. Geosci.*, 6, 597-607, 2013a

16 Regnier P., Arndt S., Goossens N., Volta C., Laruelle G. G., Lauerwald R. and Hartmann J.:  
17 Modeling estuarine biogeochemical dynamics: from the local to the global scale, *Aquat.*  
18 *Geochem.*, 19, 591-626, 2013b

19 Robinson M. C., Morris K. P. and Dyer K. R.: Deriving fluxes of suspended particulate matter  
20 in the Humber estuary, UK, using airborne remote sensing, *Mar. Pollut. Bull.*, 37, 155-163,  
21 1999

22 Ruardij P. and Van Raaphorst W.: Benthic nutrient regeneration in the ERSEM ecosystem  
23 model of the North Sea, *Neth. J. Sea Res.*, 33, 453-483, 1995

- 1 Sanford L. P. and Halka J. P.: Assessing the paradigm of mutually exclusive erosion and  
2 deposition of mud, with examples from the upper Chesapeake Bay, *Mar. Geol.*, 114, 37-57,  
3 1993
- 4 Savenije H. H. G.: A one-dimensional model for salinity intrusion in alluvial estuaries, *J.*  
5 *Hydrol.*, 85, 87-109, 1986
- 6 Savenije H. H. G.: Rapid Assessment Technique for Salt Intrusion in Alluvial Estuaries,  
7 Ph.D. Thesis, IHE Report Series 27, International Institute for Infrastructure, Hydraulics and  
8 Environment, Delft, The Netherlands, 1992
- 9 Savenije H. H. G.: A simple analytical expression to describe tidal damping or amplification,  
10 *J. Hydrol.*, 243, 205-215, 2001
- 11 Savenije H. H. G.: *Salinity and Tides in Alluvial Estuaries*, 1st edition, Elsevier, Amsterdam,  
12 The Netherlands, 2005
- 13 Savenije H. H. G. and Veling E. J. M.: Relation between tidal damping and wave celerity in  
14 estuaries, *J. Geophys. Res.*, 110, 1-10, 2005
- 15 Savenije H. H. G.: *Salinity and Tides in Alluvial Estuaries*, 2nd edition, available at:  
16 <http://salinityandtides.com>, 2012
- 17 **Slomp C. P. and Van Cappellen P.: The global marine phosphorus cycle: sensitivity to**  
18 **oceanic circulation, *Biogeosciences*, 4, 155–171, doi:10.5194/bg-4-155-2007, 2007.**
- 19 Soetaert K. and Herman P. M. J.: Estimating estuarine residence times in the Westerscheldt  
20 (The Netherlands) using a box model with fixed dispersion coefficients, *Hydrobiologia*, 311,  
21 215-224, 1995
- 22 Soetaert K., Herman P. M. J. and Middelburg J. J.: A model of early diagenetic processes  
23 from the shelf to abyssal depths, *Geochim. Cosmochim. Ac.*, 60, 1019-1040, 1996

- 1 Soetaert K., Middelburg J. J., Heip C., Meire P., Van Damme S. and Maris T.: Long-term  
2 change in dissolved inorganic nutrients in the heterotrophic Scheldt estuary (Belgium, The  
3 Netherlands), *Limnol. Oceanog.*, 51, 409-423, 2006
- 4 Stigter C. and Siemons J.: Calculation of longitudinal salt distribution in estuaries as function  
5 of time, Publication Delft Hydraulics Laboratory 52, The Netherlands, 1967
- 6 Stommel H. and Farmer G.: Abrupt change in width in two-layer open channel flow, *J.*  
7 *Marine Res.*, 11, 205-214, 1952
- 8 Stumm W. and Morgan J. J.: *Aquatic Chemistry*, 3rd edition, John Wiley & Sons, New York,  
9 1996
- 10 Stumpf R. P.: Sediment Transport in Chesapeake Bay During Floods: Analysis Using Satellite  
11 and Surface Observations, *J. Coastal Res.*, 4, 1-15, 1988
- 12 Syed T. H., Famiglietti J. S. and Chambers D. P.: GRACE-Based Estimates of Terrestrial  
13 Freshwater Discharge from Basin to Continental Scales, *J. Hydrometeorol.*, 10, 22-40, 2008
- 14 Thieu V., Mayorga E., Billen G., Garnier J.: Sub-Regional and Downscaled-Global Scenarios  
15 of Nutrient Transfer in River Basins: the Seine-Scheldt-Somme Case Study, Special issue  
16 "Past and Future Trends in Nutrient Export from Global Watersheds and Impacts on Water  
17 Quality and Eutrophication, *Global Biogeochem. Cy.*, 24, 1-15, 2010
- 18 Thouvenin B., Le Hir P. and Romana L. A.: Dissolved oxygen model in the Loire Estuary, in:  
19 *Changes in Fluxes in Estuaries: Implications from Science to Management*, Dyer K. R. and  
20 Orth R. J. (Ed.), Olsen and Olsen, Fredensborg, 169-178, 1994
- 21 Van Damme S., Struyf E., Maris T., Ysebaert T., Dehairs F., Tackx M., Heip C. and Meire P.:  
22 Spatial and temporal patterns of water quality along the estuarine salinity gradient of the

1 Scheldt estuary (Belgium and The Netherlands): results of an integrated monitoring approach,  
2 *Hydrobiologia*, 540, 29-45, 2005

3 Van der Burgh P.: Ontwikkeling van een methode voor het voorspellen van zoutverdelingen  
4 in estuaria, kanalen and zeeën, Rijkswaterstaat Rapport, The Netherlands, 1972

5 van der Goot E.: Technical description of interpolation and processing of meteorological data  
6 in CGMS, Technical Report, Space Applications Institute, Joint Research Centre of the EU,  
7 Ispra, Italy, 1997

8 van der Wal D., van Kessel T., Eleveld M. A. and Vanlede J.: Spatial heterogeneity in  
9 estuarine mud dynamics, *Ocean Dynam.*, 60, 519-533, 2010

10 Van der Zee C., Roevros N. and Chou L.: Phosphorus speciation, transformation and retention  
11 in the Scheldt estuary (Belgium/The Netherlands) from the freshwater tidal limits to the North  
12 Sea, *Mar. Chem.*, 106, 76-91, 2007

13 van Ledden M., van Kesteren W. G. M. and Winterwerp J. C.: A conceptual framework for  
14 the erosion behaviour of sand-mud mixtures, *Cont. Shelf Res.*, 24, 1-11, 2004

15 Vanderborgh J. P., Wollast R., Loijens M. and Regnier P.: Application of a transport-reactive  
16 model to the estimation of biogas fluxes in the Scheldt estuary, *Biogeochemistry*, 59, 207-  
17 237, 2002

18 Vanderborgh J. P., Folmer I., Aguilera D. R., Uhrenholdt T. and Regnier P.: Reactive-  
19 transport modelling of a river-estuarine-coastal zone system: application to the Scheldt  
20 estuary, *Mar. Chem.*, 106, 92-110, 2007

21 Weger H. G., Herzig R., Falkowski P. G. and Turpin D. H.: Respiratory losses in the light in a  
22 marine diatom: measurements by short-term mass spectrometry, *Limnol. Oceanog.*, 34, 1153-  
23 1161, 1989

- 1 Winterwerp J. C.: On the flocculation and settling velocity of estuarine mud, *Cont. Shelf Res.*  
2 22, 1339-1360, 2002
- 3 Wolanski E., Gibbs R. J., Mazda Y., Mehta A. and King B.: The role of turbulence in the  
4 settling of mud flocs, *J. Coastal Res.*, 8, 35-46, 1992
- 5 Wollast R. and Peters J. J: Biogeochemical properties of an estuarine system: the river  
6 Scheldt, in: *Proceedings of a UNESCO/SCOR Workshop on Biogeochemistry of estuarine*  
7 *sediments, Melreux, Belgium, 1976, 3-86, 1978*
- 8 Wollast R. and Marijns A.: Evaluation des contributions de différentes sources de matière en  
9 suspension à l'envasement de l'Escaut, Final report to the Ministry of Public Health and  
10 Environment, Belgium, 1981
- 11 World Ocean Atlas: <http://www.nodc.noaa.gov/OC5/indprod.html>, last access: 11 June 2012  
12

1 Table 1. Biological formulations and stoichiometric equations used in the C-GEM  
2 biogeochemical reaction network.  $T_{abs}$  and  $T$  denote the absolute and the Celsius  
3 temperature, respectively, and  $H$  is the water depth. <sup>(a)</sup> Vanderborgh et al., 2007; <sup>(b)</sup> Arndt et  
4 al., 2009; <sup>(c)</sup> Garnier et al., 1995. \*If PHY=DIA,  $nlim$  needs to account for the silica  
5 limitation for the phytoplankton growth

Gross Primary Production <sup>(a)</sup>	$GPP = P_{max}^B \cdot nlim \cdot PHY \cdot \int_H^0 1 - \exp\left(-\frac{\alpha}{P_{max}^B} \cdot I(0) \cdot \exp(-K_D \cdot H)\right) dz$
Net Primary Production <sup>(a)</sup>	$NPP = \frac{GPP}{H} \cdot (1 - k_{excr}) \cdot (1 - k_{growth}) - k_{maint} \cdot PHY$
Phytoplankton mortality <sup>(a)</sup>	$phy\_death = k_{mort}(T) \cdot PHY$
Aerobic degradation <sup>(a)</sup>	$Aer\_deg = k_{ox} \cdot f_{het}(T_{abs}) \cdot \frac{TOC}{TOC + K_{TOC}} \cdot \frac{O_2}{O_2 + K_{O_2}}$
Denitrification <sup>(a)</sup>	$Denit = k_{denit} \cdot f_{het}(T_{abs}) \cdot \frac{TOC}{TOC + K_{TOC}} \cdot \frac{NO_3}{NO_3 + K_{NO_3}} \cdot \frac{K_{in,O_2}}{O_2 + K_{in,O_2}}$
Nitrification <sup>(a)</sup>	$Nit = k_{nit} \cdot f_{nit}(T_{abs}) \cdot \frac{NH_4}{NH_4 + K_{NH_4}} \cdot \frac{O_2}{O_2 + K_{O_2}}$
Oxygen air exchange <sup>(a)</sup>	$O_{2,ex} = \frac{vp}{H} \cdot (O_{2,sat} - O_2)$
Maximum photosynthesis rate <sup>(b)</sup>	$P_{max}^B = \frac{1}{\theta} \cdot \exp(0.33 + 0.102 \cdot T)$
Nutrients limitation for phytoplankton growth <sup>(c), *</sup>	$nlim = \frac{NO_3 + NH_4}{NO_3 + NH_4 + K_N} \cdot \frac{PO_4}{PO_4 + K_{PO_4}}$
Light extinction coefficient <sup>(a)</sup>	$K_D = K_{D1} + K_{D2} \cdot SPM$
Piston velocity <sup>(a)</sup>	$vp = k_{flow} + k_{wind}$

Temperature dependences for biogeochemical processes <sup>(b)</sup>

$$f_{het}(T_{abs}) = 2.75^{\left(\frac{T_{abs}-278}{10}\right)} \quad ; \quad f_{nit}(T_{abs}) = 5^{\left(\frac{T_{abs}-278}{10}\right)}$$

Current component for  $\nu p$  <sup>(a)</sup>

$$k_{flow} = \sqrt{\frac{U \cdot D_{O_2}(T_{abs})}{H}}$$

Wind component for  $\nu p$  <sup>(a)</sup>

$$k_{wind} = \frac{1}{3.6 \cdot 10^5} \cdot 0.31 \cdot U_{wind,10m}^2 \cdot \sqrt{\frac{Sc(T,S)}{660}}$$

Switch between  $NH_4$  and  $NO_3$  utilization <sup>(a)</sup>

$$f_{NH_4} = \frac{NH_4}{10 + NH_4}$$

$$dPHY/dt = NPP - phy\_death$$

$$dSi/dt = -redsi \cdot NPP$$

$$dTOC/dt = -Aer\_deg - Denit + phy\_death$$

$$dNO_3/dt = -94.4/106 \cdot Denit - redn \cdot (1 - f_{NH_4}) \cdot NPP + Nitr$$

$$dNH_4/dt = redn \cdot (R - f_{NH_4} \cdot NPP) - Nitr$$

$$dO_2/dt = -Aer\_deg + f_{NH_4} \cdot NPP + 138/106 \cdot (1 - f_{NH_4}) \cdot NPP - 2 \cdot Nitr + O_{2,ex}$$

$$dPO_4/dt = redp \cdot (Aer\_deg + Denit - NPP)$$

1 Table 2. Values for physical parameters used in C-GEM for stationary and transient  
 2 simulations.

<b>Physical parameters</b>		
Name	Description	Value
$H_0$	Depth at the estuarine mouth [m]	11.5
$B_0$	Width at the estuarine mouth [m]	6952
$b$	Width convergence length [m]	29014
$H_{MW}$	Average tidal amplitude [m]	3.7
$P$	Tidal prism [m <sup>3</sup> ]	1200·10 <sup>6</sup>
$T$	Tidal period [s]	45720
$Q_b$	Bankfull discharge [m <sup>3</sup> ]	500
$\bar{H}$	Average water depth [m]	6.7

3

1 Table 3. Boundary conditions and external forcings for the steady-state simulation. <sup>(a)</sup> Arndt  
 2 et al., 2007; <sup>(b)</sup> Vanderborcht et al., 2007; <sup>(c)</sup> Van der Zee et al., 2007; <sup>(d)</sup> Typical value for a  
 3 summer period in Belgium (IRM, 2004)

<b>Boundary conditions</b>				
	Sea	Scheldt	Rupel	Unit
SPM <sup>(a)</sup>	0.03	0.07	-	g l <sup>-1</sup>
TOC <sup>(b)</sup>	0	393	1864.6	μM C
NO <sub>3</sub> <sup>(b)</sup>	50	198	55.3	μM N
NH <sub>4</sub> <sup>(b)</sup>	0	520	884.2	μM N
PO <sub>4</sub> <sup>(c)</sup>	0	17	8.3	μM P
O <sub>2</sub> <sup>(b)</sup>	250	106	74.4	μM O <sub>2</sub>
Diatoms <sup>(b)</sup>	10	50	0	μM C
dSi <sup>(b)</sup>	10	250	250	μM Si
<b>External forcings</b>				
	Sea	Scheldt	Rupel	Unit
Discharge <sup>(b)</sup>	-	32	32.7	m <sup>3</sup> s <sup>-1</sup>
Temperature <sup>(b)</sup>		17		°C
Light intensity	Calculated as in Billen et al. (1994) using an average cloud coverage of 60% <sup>(d)</sup>			μE m <sup>-2</sup> s <sup>-1</sup>

4

1 Table 4. Values for biogeochemical parameters used in C-GEM for stationary and transient  
 2 simulations. All rates are defined at 278.15 K. <sup>(a)</sup> from Vanderborcht et al., 2007. <sup>(b)</sup> from  
 3 Billen and Garnier, 1997. All other values are from Arndt et al., 2009

Biogeochemical parameters				
Name	Description	Unit	Value	
			Stationary simulation	Transient simulation
$P_{\max}^B$	Maximum specific photosynthetic rate	$s^{-1}$	$1.16 \cdot 10^{-4}$ <sup>(a)</sup>	Calculated
$\alpha$	Photosynthetic efficiency	$m^2 s (\mu E s)^{-1}$	$5.8 \cdot 10^{-7}$	$5.8 \cdot 10^{-7}$
$\theta$	Ratio of gram carbon to gram chlorophyll a	$gC gChla^{-1}$	-	50
$K_{DSi}$	Michaelis-Menten constant for dissolved silica	$\mu M Si$	20	20
$K_{PO4}$	Michaelis-Menten constant for phosphate <sup>(b)</sup>	$\mu M P$	0.5	0.5
$K_{NH4}$	Michaelis-Menten constant for ammonium	$\mu M N$	100	100
$K_{NO3}$	Michaelis-Menten constant for nitrate	$\mu M N$	45	45
$K_{TOC}$	Michaelis-Menten constant for organic matter	$\mu M C$	60	60
$K_{O2}$	Michaelis-Menten constant for oxygen	$\mu M O_2$	15	15
$K_N$	Michaelis-Menten constant for dissolved nitrogen	$\mu M N$	5	5
$K_{in,O2}$	Inhibition term for denitrification	$\mu M O_2$	50	50
$redsi$	Redfield ratio for silica	$mol Si mol C^{-1}$	16/80	16/80
$redn$	Redfield ratio for nitrogen	$mol N mol C^{-1}$	16/106	16/106
$redp$	Redfield ratio for phosphorous	$mol P mol C^{-1}$	1/106	1/106

		C <sup>-1</sup>		
$k_{maint}$	Maintenance rate constant	s <sup>-1</sup>	$9.26 \cdot 10^{-7}$	$9.26 \cdot 10^{-7}$
$k_{mort}$	Mortality rate constant	s <sup>-1</sup>	$7.1 \cdot 10^{-7}$	$7.1 \cdot 10^{-7}$
$k_{excr}$	Excretion constant	-	0.03	0.03
$k_{growth}$	Growth constant	-	0.3	0.3
$K_{D1}$	Background extinction coefficient	m <sup>-1</sup>	1.3	1.3
$K_{D2}$	Specific attenuation of suspended matter	(mg.m) <sup>-1</sup>	0.06	0.06
$k_{ox}$	Aerobic degradation rate constant	μM C s <sup>-1</sup>	$2 \cdot 10^{-4}$	$2 \cdot 10^{-4}$
$k_{denit}$	Denitrification rate constant	μM C s <sup>-1</sup>	$1 \cdot 10^{-4}$	$1 \cdot 10^{-4}$
$k_{nit}$	Nitrification rate constant	μM N s <sup>-1</sup>	$1.5 \cdot 10^{-4}$	$1.5 \cdot 10^{-4}$

1

1 Table 5. Calibrated sediment parameters used in C-GEM for stationary and transient  
 2 simulations. Note that a linear variation is applied to the Chezy coefficient ( $C$ ) and the  
 3 critical shear stress for erosion and deposition ( $\tau_{cr}$ ) between km 100 and km 158 is applied.  
 4 Numerical values assigned to  $C_{158km}$  and  $\tau_{cr,158km}$  correspond to their value imposed at the  
 5 estuarine upper boundary.

Sediment parameters		
Name	Description [unit]	Value
$g$	Acceleration due to gravity [ $m\ s^{-2}$ ]	9.81
$C$	Chézy coefficient [ $m^{1/2}\ s^{-1}$ ]	$C_{0-100km} = 70$ ; $C_{158km} = 40^*$
$\rho_w$	Density of pure water [ $kg\ m^{-3}$ ]	1000
$w_s$	Settling velocity [ $m\ s^{-1}$ ]	$1 \cdot 10^{-3}$
$\tau_{cr}$	Critical shear stress for erosion and deposition [ $N\ m^{-2}$ ]	$\tau_{cr,0-100km}=0.4$ ; $\tau_{cr,158km}=1.0^*$
$E$	Erosion coefficient [ $kg\ m^{-2}\ s^{-1}$ ]	$E_{0-100km}=3.5 \cdot 10^{-6}$ ; $E_{100-158km}=6.0 \cdot 10^{-8}$

6

1 Table 6. Lateral loads [ $\text{mmol s}^{-1}$ ]. For more information, refer to Vanderborght et al. (2007)  
 2 and Arndt et al. (2009)

Location			TOC		NH <sub>4</sub>		NO <sub>3</sub>	
Distance	from	the	Stationary	Transient	Stationary	Transient	Stationary	Transient
estuarine mouth [km]			simulation	simulation	simulation	simulation	simulation	simulation
2			2247	0	972	0	897	0
23			7349	0	11511	0	3370	0
34			1356	0	847	0	435	0
45			571	0	847	0	951	0
57			143	0	174	0	435	0
65			2640	0	2442	0	2202	0
74			6742	2450	2516	1132	1277	0
84			3674	747	2018	530	1767	0
90			4281	14208	1221	6670	299	0
97			6421	3536	2018	1561	639	0
110			0	2616	0	1068	0	0
118			0	593	0	199	0	0
141			0	4444	0	1708	0	0
157			0	1757	0	1123	0	0

3

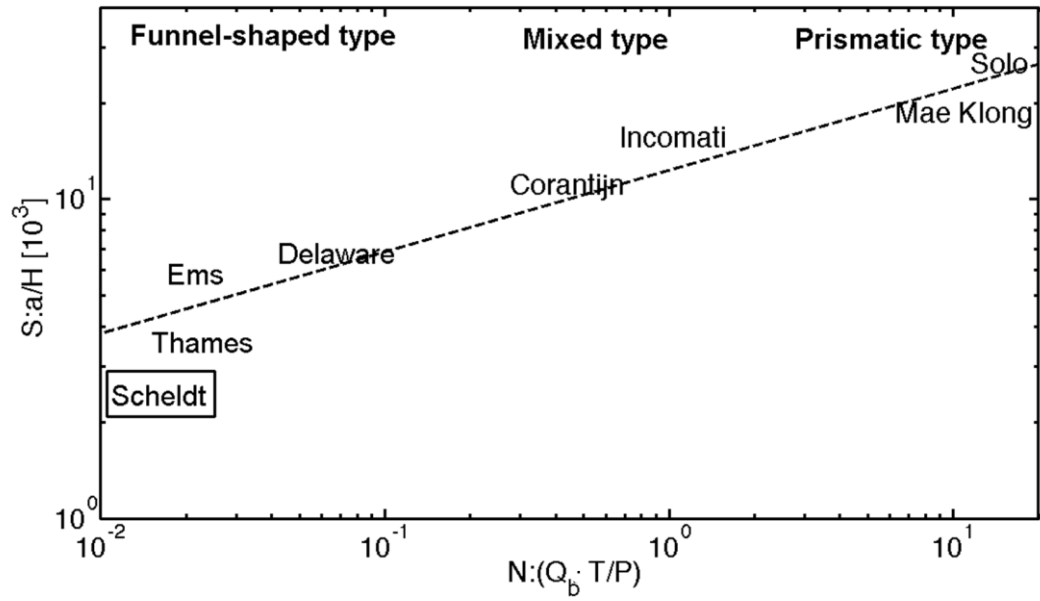
- 1 Table 7. List of parameter values for the reference case and percentage of variation applied
- 2 to perform the sensitivity tests.

Parameter		Reference value	Variation [%]
Geometric parameters	$LC$ = convergence length [m]	29014	$\pm 10$
	$H$ = water depth [m]	Variable	$\pm 20$
Sediment parameters	$E$ = erosion coefficient [ $\text{mg m}^2 \text{s}^{-1}$ ]	Variable	$\pm 50$
	$\tau_{cr}$ = critical shear stress for erosion and deposition [ $\text{N m}^{-2}$ ]	Variable	$\pm 50$
	$C$ = Chézy coefficient [ $\text{m}^{1/2} \text{s}^{-1}$ ]	Variable	$\pm 50$
	$W_s$ = settling velocity [ $\text{m s}^{-1}$ ]	$1 \cdot 10^{-3}$	$\pm 50$
Primary production parameters	$\alpha$ = photosynthesis efficiency [ $\text{m}^2 \text{s}^{-1} \mu\text{E}^{-1}$ ]	$5.8 \cdot 10^{-7}$	$\pm 50$
	$k_{excr}$ = excretion constant [-]	0.03	$\pm 50$
	$k_{growth}$ = growth constant [-]	0.3	$\pm 50$
	$k_{maint}$ = maintenance rate constant [ $\text{s}^{-1}$ ]	$9.26 \cdot 10^{-7}$	$\pm 50$
	$k_{mort}$ = mortality rate constant [ $\text{s}^{-1}$ ]	$7.1 \cdot 10^{-7}$	$\pm 50$
Biogeochemical reaction rates	$k_{nit}$ = nitrification rate constant [ $\mu\text{M N s}^{-1}$ ]	$1.5 \cdot 10^{-4}$	$\pm 50$
	$k_{ox}$ = aerobic degradation rate	$2.0 \cdot 10^{-4}$	$\pm 50$

			constant [ $\mu\text{M C s}^{-1}$ ]		
			$k_{denit}$ = denitrification rate constant [ $\mu\text{M C s}^{-1}$ ]	$1.0 \cdot 10^{-4}$	$\pm 50$
O <sub>2</sub>	air	exchange	$k_{flow}$ = current component for piston velocity [ $\text{m s}^{-1}$ ]	Variable	$\pm 50$
parameter					

1

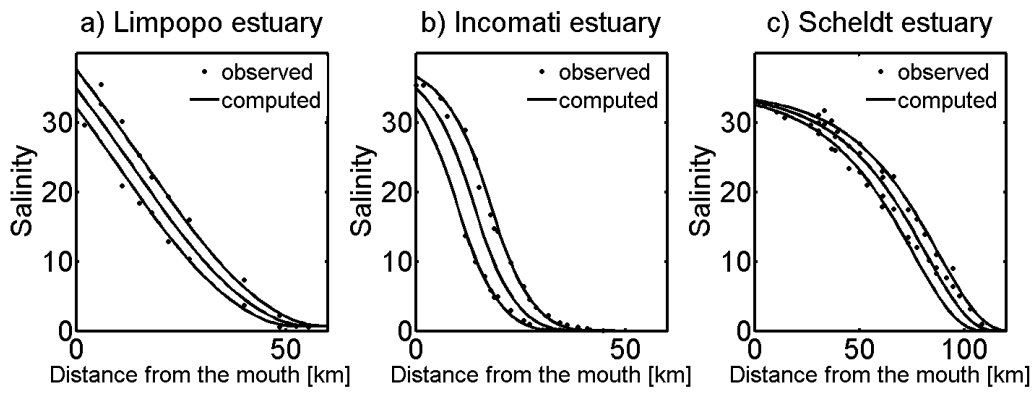
2



1

2 Figure 1. Relationship between geometric (S) and hydrodynamic (N) characteristics of  
 3 alluvial estuaries (modified from Savenije, 1992). The Scheldt estuary, where C-GEM has  
 4 been tested, is highlighted.

5

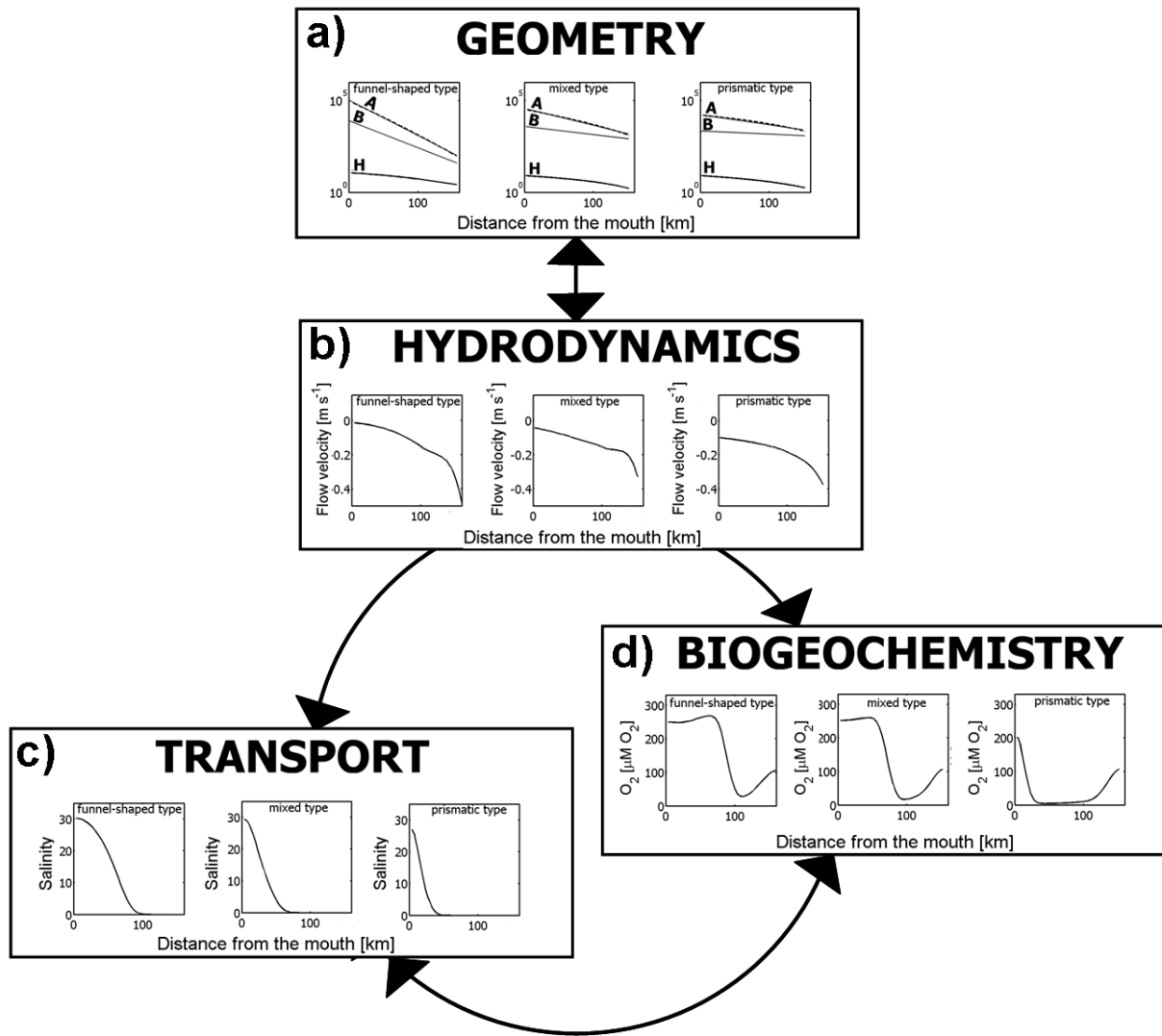


1

2 Figure 2. Measured (dots) and simulated (line) longitudinal salinity distribution at high water  
 3 slack, low water slack and for tidal average conditions for the three main types of alluvial  
 4 estuaries: a) Limpopo (prismatic), b) Incomati (mixed type) and c) Scheldt (funnel-shaped).

5 All data are available at <http://salinityandtides.com>.

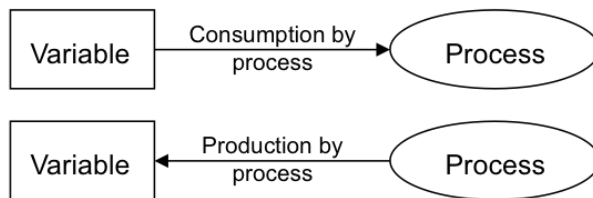
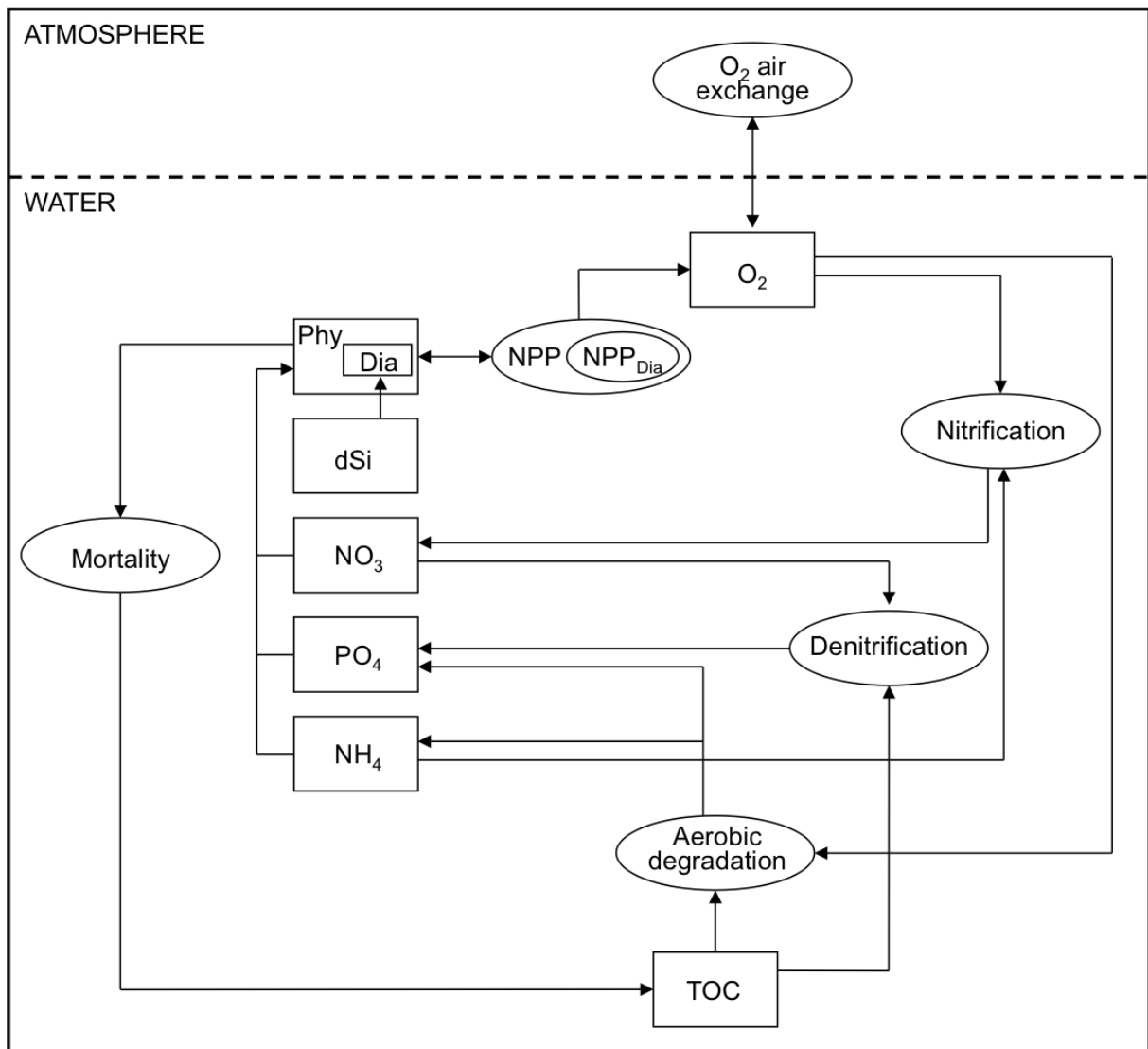
6



1

2 Figure 3. The C-GEM concept. Each estuarine type responds in a typical manner to the  
 3 interdependence between geometry and hydrodynamics and to the first-order control of  
 4 hydrodynamics on estuarine biogeochemistry. Longitudinal distribution of: a) A=cross-  
 5 section area in  $\text{m}^2$ ; B=width in m; H=water depth in m; b) flow velocity in  $\text{m s}^{-1}$ ; c) salinity;  
 6 d)  $\text{O}_2$  concentration in  $\mu\text{M O}_2$ .

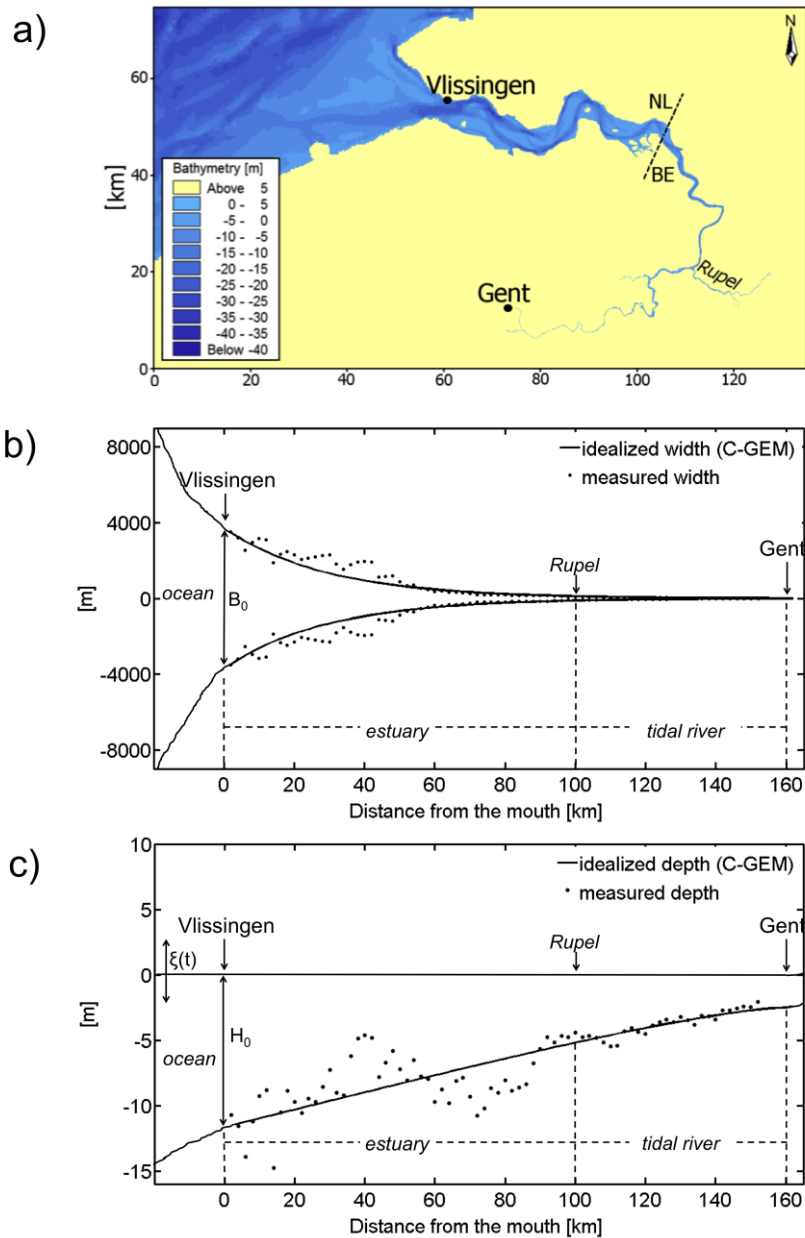
7



1

2 Figure 4. Conceptual scheme of the biogeochemical module of C-GEM, as used in our  
 3 applications to the Scheldt estuary (see Section 4). State-variables and processes are  
 4 represented by boxes and circles, respectively. DIA corresponds to diatoms.

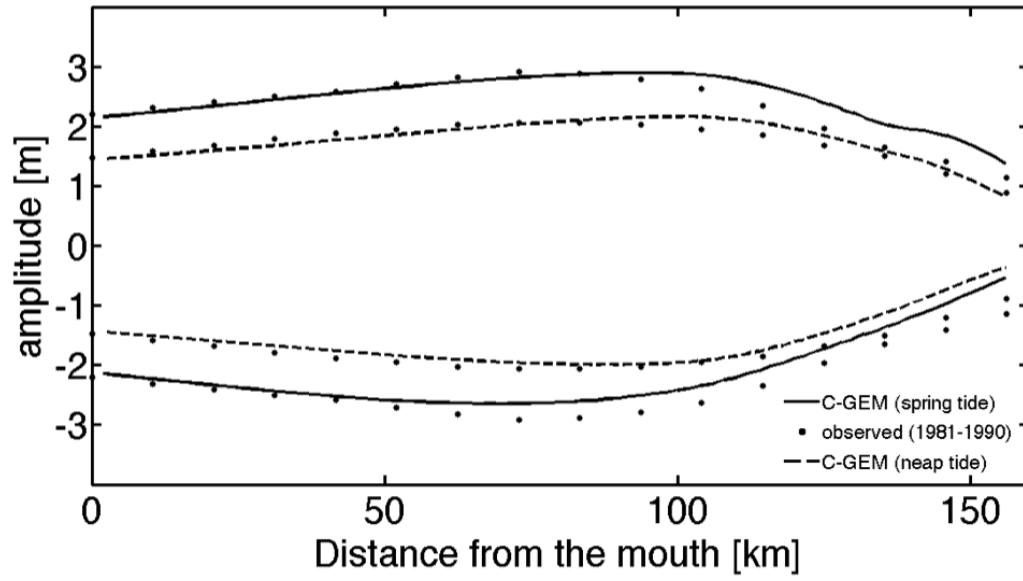
5



1

2 Figure 5. **Panel a: Map** of the Scheldt estuary obtained with a horizontal resolution of  
 3 80m×80m for the channel up to the Belgian/Dutch border and of 250m×250m for the lower  
 4 estuary. **Panels b and c: Comparison between observed width and depth (dots) and the**  
 5 **idealized geometry supporting C-GEM (thick lines).** The estuarine mouth is located at  
 6 Vlissingen.

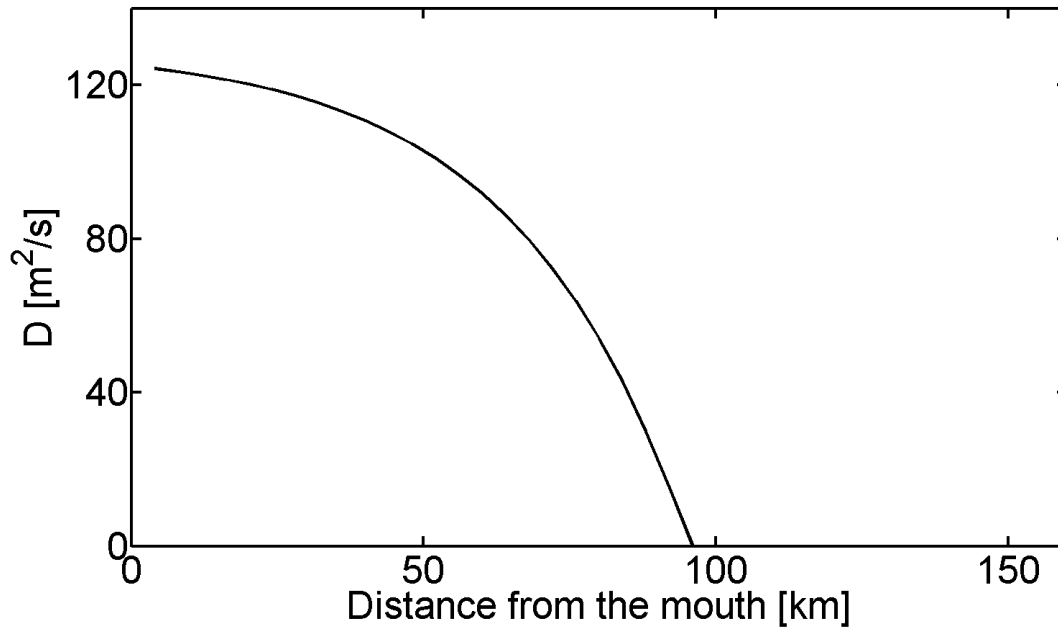
7



1

2 Figure 6. Comparison between observed (1981-1990) (dots) and simulated neap (dashed  
 3 line) and spring (solid line) tidal amplitudes modelled using a constant freshwater discharge  
 4  $Q=100 \text{ m}^3 \text{ s}^{-1}$ .

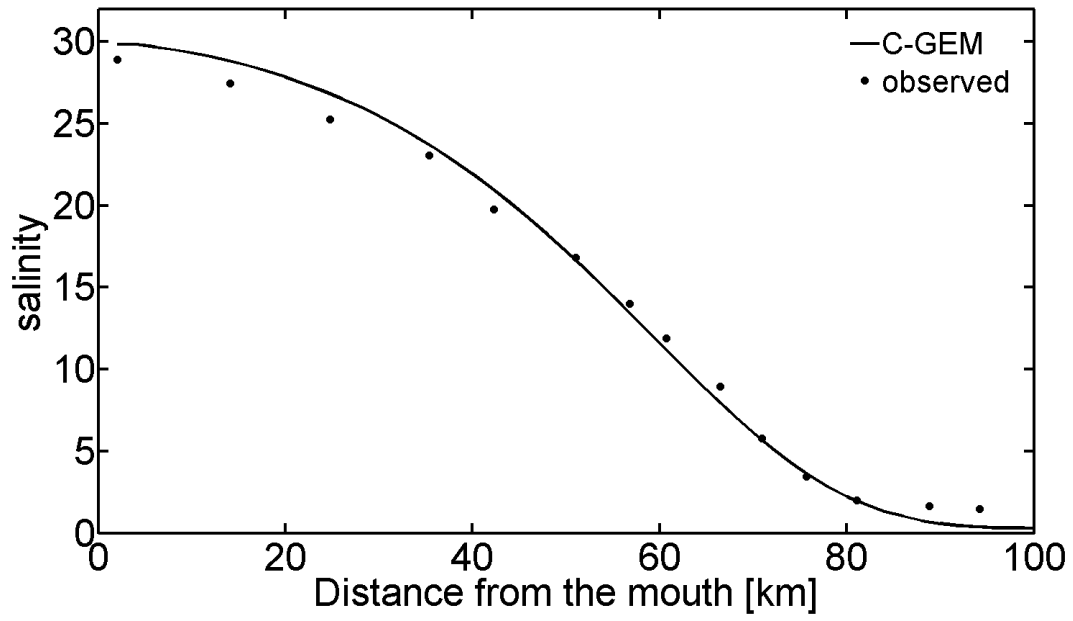
5



1

2 Figure 7. Longitudinal dispersion coefficient distribution modelled using a constant  
3 freshwater discharge  $Q=39 \text{ m}^3 \text{ s}^{-1}$  and a Van der Burgh's coefficient  $K$  of 0.39.

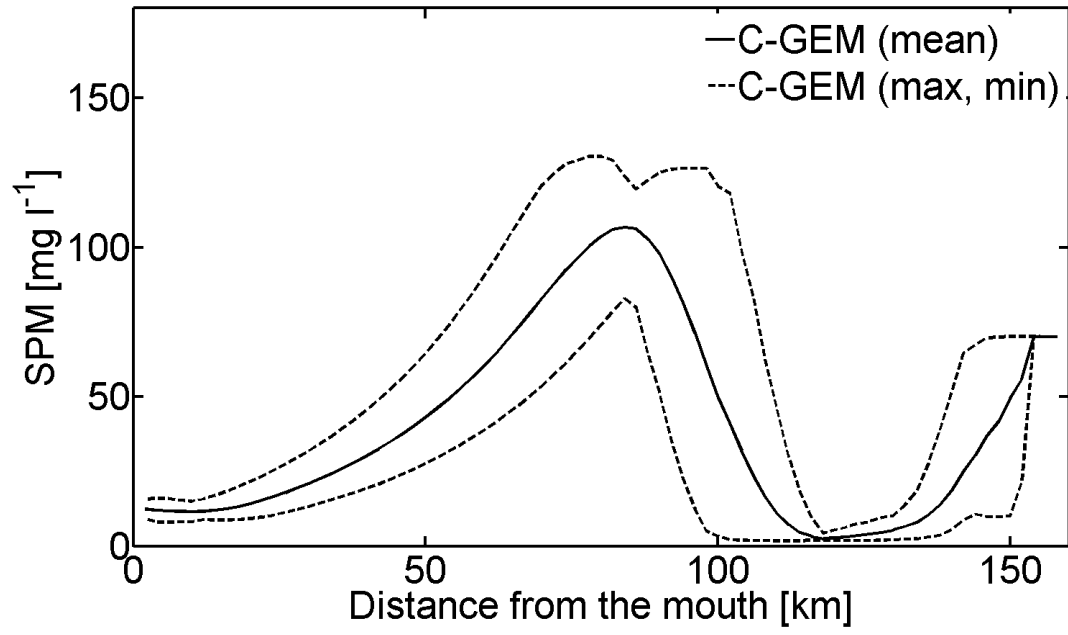
4



1

2 Figure 8. Comparison between salinity measurements (Regnier et al., 1998) and simulated  
3 longitudinal distribution of the tidally averaged salinity for a mean tidal amplitude of 3.7m,  
4 modelled using a constant freshwater discharge  $Q=39 \text{ m}^3 \text{ s}^{-1}$ .

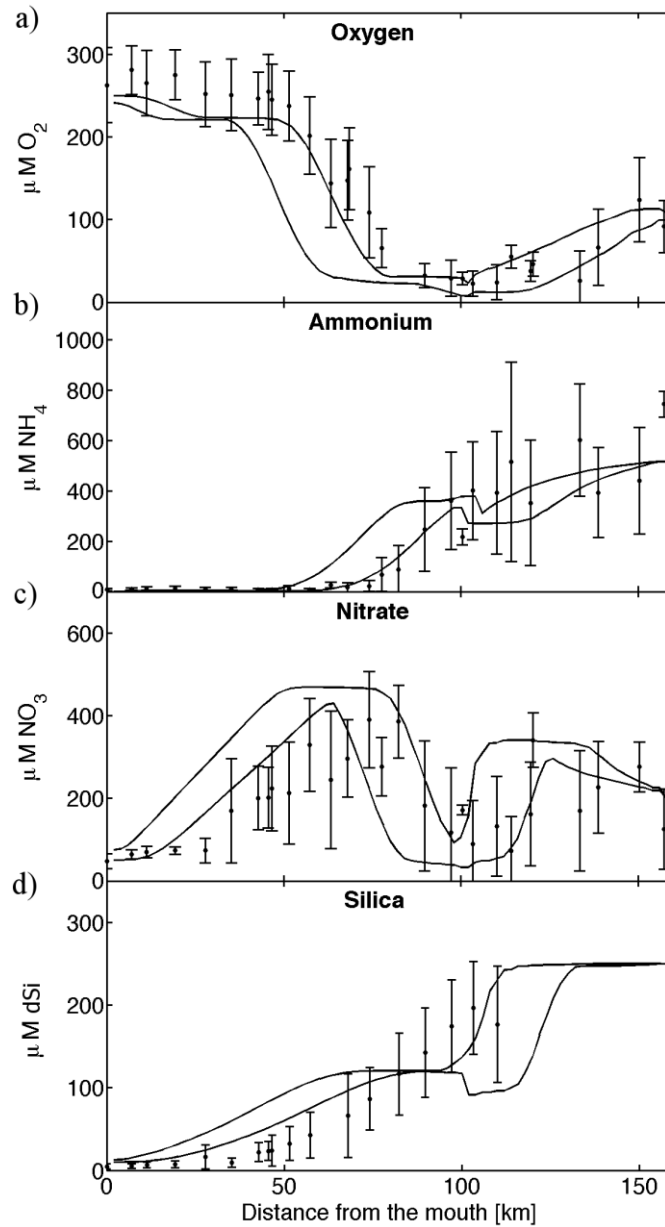
5



1

2 Figure 9. Mean, maximum and minimum longitudinal distribution of SPM concentrations for  
 3 a constant river discharge  $Q=39 \text{ m}^3 \text{ s}^{-1}$ . Parameters and conditions are listed in Tables 2-4.

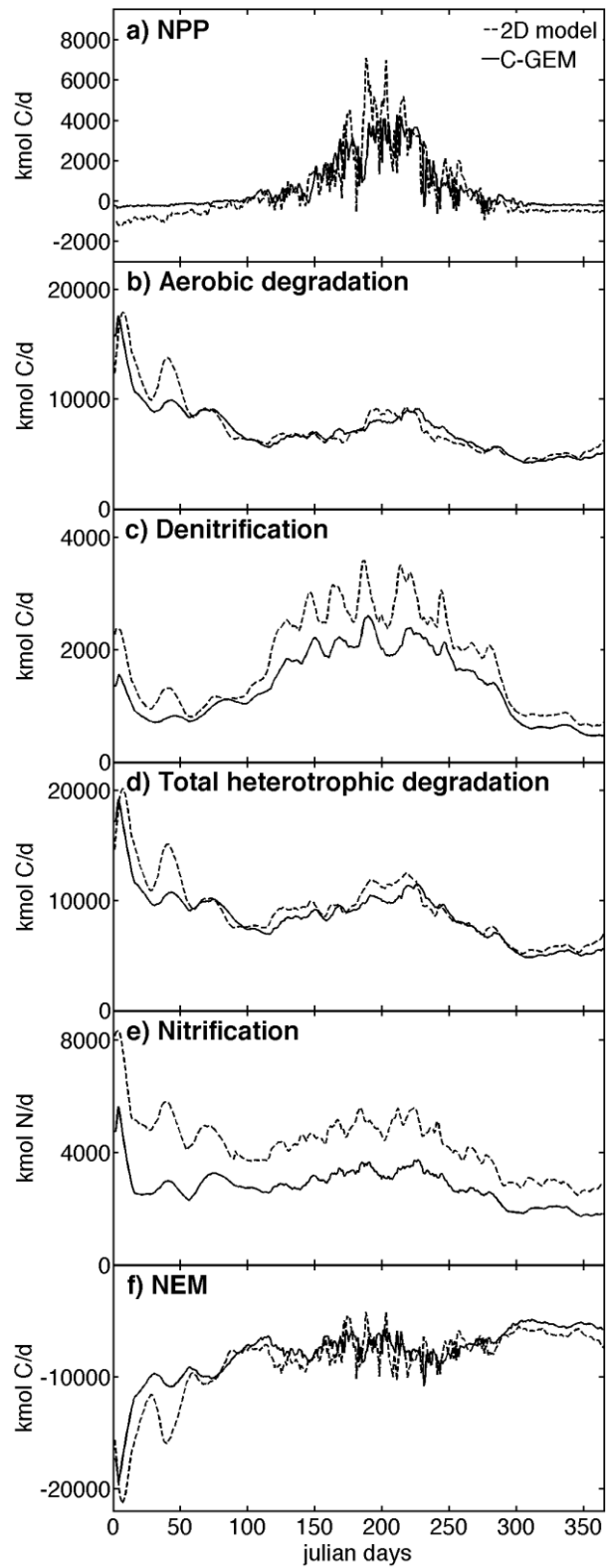
4



1

2 Figure 10. Comparison between longitudinal distributions of field data averaged over the  
 3 period May-September for the years 1990-1995 (dots; vertical bars correspond to the  
 4 standard deviation) and steady-state maximum and minimum  $O_2$ ,  $NH_4$ ,  $NO_3$  and  $dSi$   
 5 concentrations over a tidal cycle (solid line). Physical conditions are summarized in Table 2,  
 6 boundary conditions and external forcings are summarized in Table 3 and parameters are  
 7 listed in Tables 4 and 5.

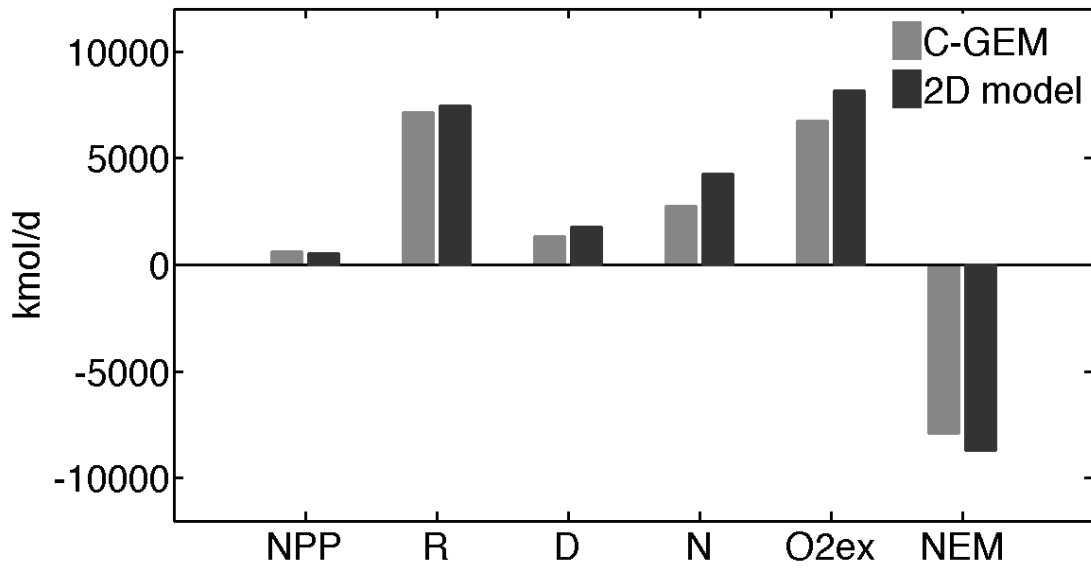
8



1

2 Figure 11. Comparison between annual evolution of biogeochemical rates modelled by C-  
 3 GEM (solid line) and the 2D-RTM (dashed line) by Arndt et al., 2009.

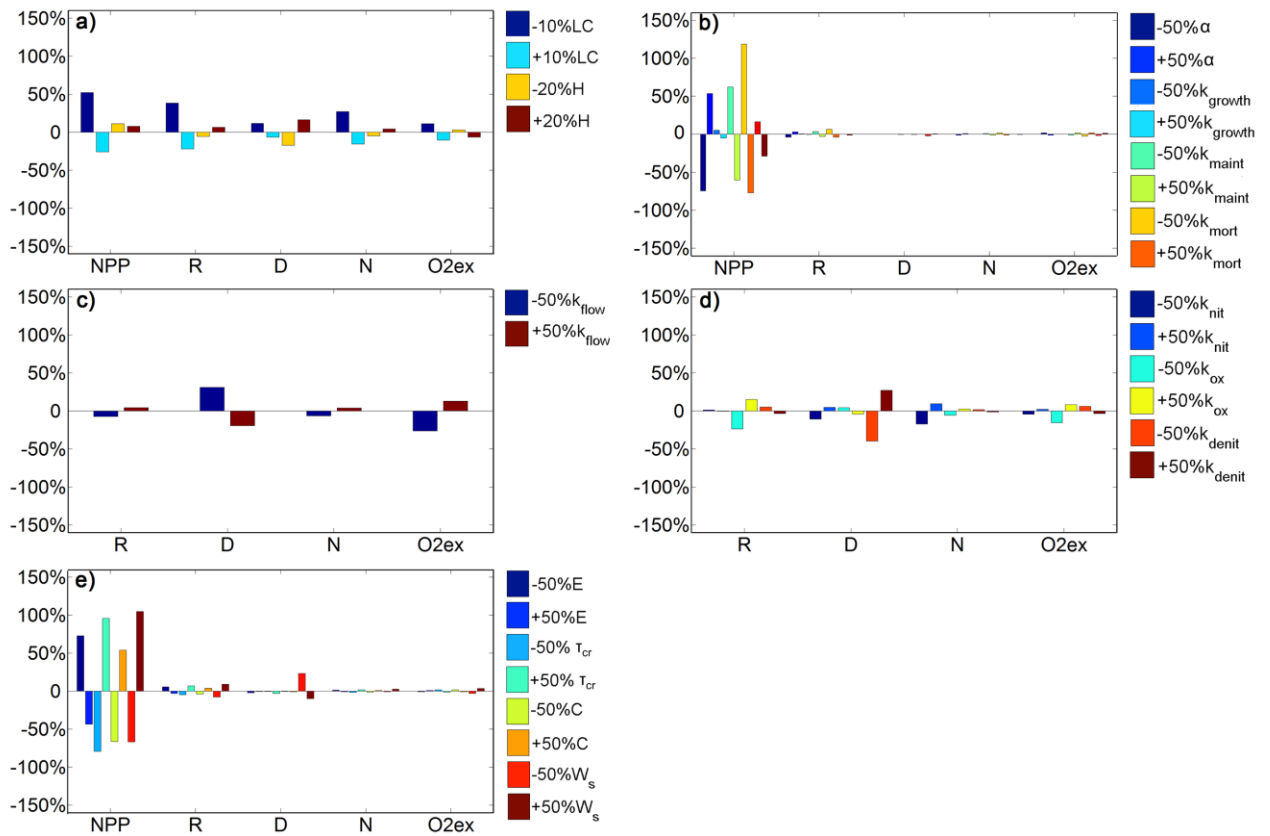
4



1

2 Figure 12. Comparison between system-integrated biogeochemical rates obtained by C-GEM  
 3 and the 2D-RTM by Arndt et al., 2009. NPP=Net Primary Production in  $\text{kmol C d}^{-1}$ ;  
 4 R=aerobic degradation in  $\text{kmol C d}^{-1}$ ; D=denitrification in  $\text{kmol C d}^{-1}$ ; N=nitrification in  
 5  $\text{kmol N d}^{-1}$ ; O2ex= $\text{O}_2$  exchange at the air-water interface in  $\text{kmol O}_2 \text{ d}^{-1}$ ; NEM=Net  
 6 Ecosystem Metabolism in  $\text{kmol C d}^{-1}$ .

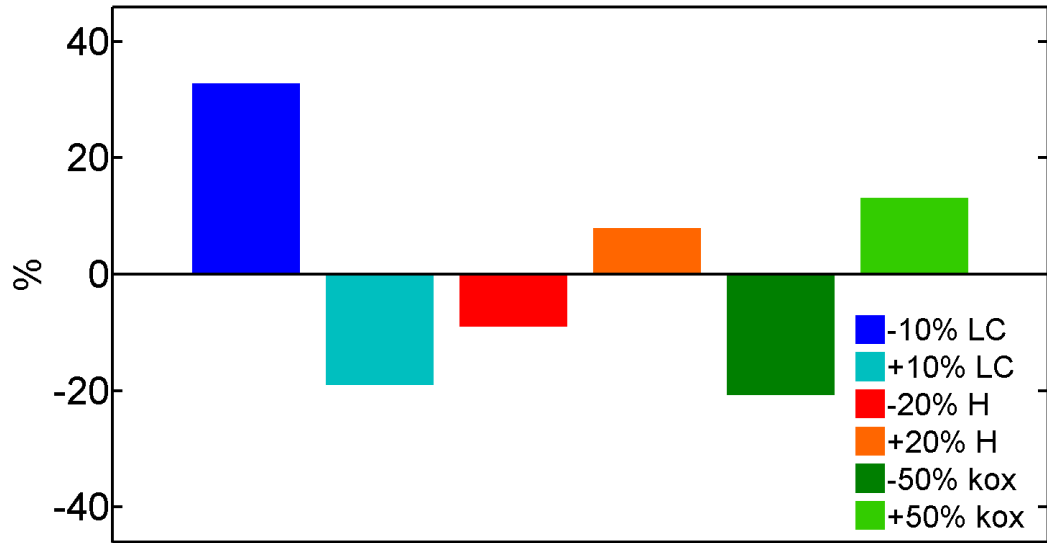
7



1

2 Figure 13. Results of sensitivity tests for variations in: (a) geometrical parameters, (b)  
 3 primary production parameters, (c) O<sub>2</sub> air exchange rate, (d) biogeochemical rate constants  
 4 and (e) sediment parameters, expressed in percent of the biogeochemical baseline budget  
 5 values (see Fig. 12).

6



1

2 Figure 14. Variations in NEM for parameters leading to a change exceeding 5% its reference

3 value (see Fig. 12).